HHS Public Access

Author manuscript

Mol Cell. Author manuscript; available in PMC 2019 January 04.

Published in final edited form as:

Mol Cell. 2018 January 04; 69(1): 87–99.e7. doi:10.1016/j.molcel.2017.11.025.

The PLAG1-GDH1 axis promotes anoikis resistance and tumor metastasis through CamKK2-AMPK signaling in LKB1-deficient lung cancer

Lingtao Jin[1,*], **Jaemoo Chun**[1], **Chaoyun Pan**[1], **Avi Kumar**[2], **Guojing Zhang**[1], **Youna Ha**[1], **Dan Li**[1], **Gina N. Alesi**[1], **Yibin Kang**[3], **Lu Zhou**[4], **Wen-Mei Yu**[5], **Kelly R. Magliocca**[6], **Fadlo R. Khuri**[1], **Qu Cheng-Kui**[1,5], **Christian Metallo**[2], **Taofeek K. Owonikoko**[1], and **Sumin Kang**[1,7,*]

[1]Department of Hematology and Medical Oncology, Winship Cancer Institute of Emory, Emory University School of Medicine, Atlanta, GA 30322, USA

[2]Department of Bioengineering, University of California San Diego, La Jolla, CA 92093, USA

[3]Department of Molecular Biology, Princeton University, Princeton, NJ 08544, USA

[4]School of Pharmacy, Fudan University, Shanghai, 201203, China

[5]Department of Pediatrics, Emory University School of Medicine, Atlanta, GA 30322, USA

[6]Department of Pathology & Laboratory Medicine, Emory University School of Medicine, Atlanta, GA 30322, USA

SUMMARY

Loss of LKB1 is associated with increased metastasis and poor prognosis in lung cancer, but the development of targeted agents is in its infancy. Here we report that a glutaminolytic enzyme glutamate dehydrogenase 1 (GDH1), upregulated upon detachment *via* pleomorphic adenoma gene 1 (PLAG1), provides anti-anoikis and pro-metastatic signals in LKB1-deficient lung cancer. Mechanistically, the GDH1 product α-KG activates CamKK2 by enhancing its substrate AMPK binding, which contributes to energy production that confers anoikis resistance. The effect of GDH1 on AMPK is evident in LKB1-deficient lung cancer, where AMPK activation predominantly depends on CamKK2. Targeting GDH1 with R162 attenuated tumor metastasis in patient-derived xenograft model and correlation studies in lung cancer patients further validated the clinical relevance of our finding. Our study provides insight into the molecular mechanism by

[*]Correspondence: lingtao.jin@emory.edu (L.J.), smkang@emory.edu (S.K.).

[7]Lead Contact: Sumin Kang, 1365C Clifton Rd NE, C3006, Emory University School of Medicine, Atlanta, GA 30322; Tel.: 404-778-1880; Fax: 404-778-5520

AUTHOR CONTRIBUTIONS

Y.K., F.R.K., C.-K.Q., and T.K.O. provided critical resources. Z.L. performed structural analyses. K.R.M. performed histopathological study. W.-M.Y. investigated the Seahorse XF assays. A.K. and C.M. performed isotope tracing. G.Z. investigated patient-derived xenograft. L.J., J.C., C.P., Y.H. D.L., and G.N.A. performed all other experiments. L.J. did project administration and data analysis of the study. S.K. supervised the study and wrote the paper.

which GDH1-mediated metabolic reprogramming of glutaminolysis mediates lung cancer metastasis and offers a therapeutic strategy for patients with LKB1-deficient lung cancer.

Graphical Abstract

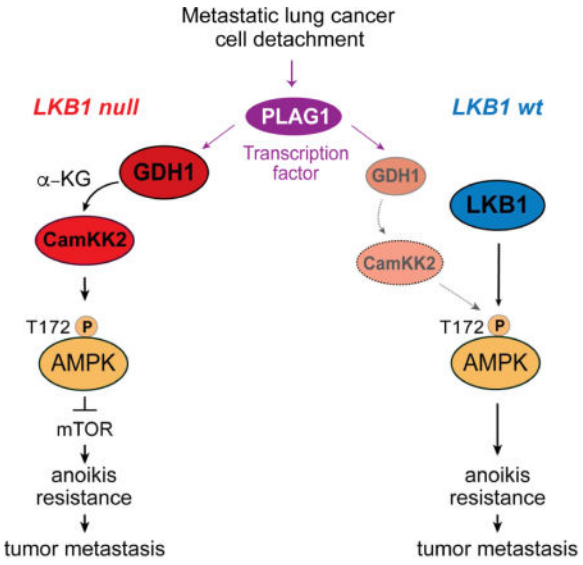

INTRODUCTION

Tumor metastasis is a major contributor to deaths from nearly all types of cancers (Steeg, 2016). The metastatic cascade represents a multi-step biological process (Fidler, 2003; Gupta and Massague, 2006). Anoikis, which is a form of programmed cell death resulting from loss of cell and extracellular membrane interaction, is known as a physiological barrier to metastasis (Fidler, 2003; Paoli et al., 2013). Cancer cells must develop anoikis resistance in order to survive in the circulation before forming metastatic foci in distant organs (Kim et al., 2012; Simpson et al., 2008).

Lung cancer is the leading cause of cancer death worldwide and frequently metastasizes to distant organs. The five-year survival rate for metastatic lung cancer is only around 3% (Dela Cruz et al., 2011). 85% of lung cancer cases are non-small cell lung carcinoma (NSCLC). The development of targeted agents specifically in metastatic lung cancer is still very much in its early phase. Thus, it is critical to identify and validate promising therapeutic targets to enable significant clinical gains. About one third of lung cancer patient tumors lack or harbor inactive tumor suppressor liver kinase B1 (LKB1), and LKB1 deficiency is associated with increased metastatic rates and decreased survival in patients (Sanchez-Cespedes et al., 2002). LKB1 directly phosphorylates 5′ AMP-activated protein kinase α (AMPKα) at T172 and activates AMPK. AMPKα is also phosphorylated by other upstream kinases, calcium/calmodulin dependent protein kinase kinase 2 (CamKK2) and TGF-β-activated kinase 1 (TAK1) (Hardie et al., 2012; Luo et al., 2010). AMPK is a central regulator of cellular metabolism and energy homeostasis, which is composed of α-catalytic and two regulatory subunits β and γ (Hawley et al., 2003). AMPK contributes to pro-survival signaling by inhibiting the mTOR pathway (Avivar-Valderas et al., 2013; Kim et al.,

2011; Ng et al., 2012). AMPK can exert pro- or anti-tumorigenic roles in cancer depending on context (Faubert et al., 2015; Liang and Mills, 2013). AMPK-mediated cell survival may be critical when cancer cells are under conditions that are unfavorable for cell proliferation such as detachment from the matrix for circulation in the bloodstream during metastasis, through mechanisms that are not yet fully explored.

To generate energy and biomass for tumor growth, cancer cells are well documented to have enhanced metabolic requirements, including elevated aerobic glycolysis and glutaminolysis (Hsu and Sabatini, 2008; Kim and Dang, 2006; Warburg, 1956). We reported that activation of metabolic enzymes including pyruvate dehydrogenase kinase and 6-phosphogluconate dehydrogenase contributes to altered cancer cell metabolism and tumor growth (Hitosugi et al., 2011; Lin et al., 2015). In addition, we found that a glutaminolytic enzyme, glutamate dehydrogenase 1 (GDH1), promotes tumor growth by regulating redox homeostasis through its product α-KG and subsequent metabolite fumarate by activating an ROS scavenging enzyme glutathione peroxidase 1 (GP×1) (Jin et al., 2016; Jin et al., 2015). However, how this altered metabolism contributes to tumor metastasis and anoikis resistance remains largely unknown. While elevated aerobic glycolysis is a hallmark of proliferative cancer cells, emerging evidence suggests that disseminated metastatic tumor cells have a different metabolic phenotype compared to proliferating tumor cells (Weber, 2016). For instance, studies reveal that cancer cells switch from oxidative to reductive metabolism in utilizing glutamine during matrix detachment and support redox homeostasis *via* isocitrate dehydrogenase 1 (IDH1) (Jiang et al., 2016). Extracellular matrix (ECM) detached cells are known to be nutrient-starved which limits energy production, whereas estrogen-related receptor or oncogenes such as ErbB2 maintain TCA flux through PDK4 upregulation (Grassian et al., 2011; Kamarajugadda et al., 2012). In addition, studies show that genes associated with mitochondrial biogenesis and oxidative phosphorylation, rather than those involved in the Warburg effect, are upregulated in circulating tumor cells compared with primary tumor cells (LeBleu et al., 2014). Understanding the mechanisms underlying the metabolic changes associated with cancer spread and identifying metabolic targets that promote tumor metastasis may lead to improved clinical outcomes for patients with metastatic cancers.

Here, we uncover the molecular mechanism by which an altered tumor metabolism provides metabolic advantages to cancer cells during dissemination and contributes to tumor metastasis in lung cancer. In particular, we report that glutaminolysis, a mitochondrial pathway that consumes an alternative metabolic substrate glutamine, contributes to anti-anoikis and pro- metastatic signaling through GDH1 and its product α-KG by activating the CamKK2-mediated AMPK signaling pathway.

RESULTS

GDH1 is upregulated in detached metastatic human lung cancer cells

To better understand the link between glutaminolysis and tumor metastasis, we first screened for a factor in the glutaminolysis pathway that contributes to the acquisition of anoikis resistance, the prerequisite for metastasis. We induced anoikis by culturing cells under detached conditions and monitored any expression changes in glutaminolytic enzymes.

Among 11 enzymes tested, GDH was commonly upregulated in a panel of lung cancer cells (Figures 1A and 1B). Although the GDH primers do not distinguish the two isoforms GDH1 and GDH2, we found that GDH1 is the predominant isoform in lung cancer cells through a diagnostic restriction digest (Figure S1)(Shashidharan et al., 1994). We next examined the effect of blocking glutamine metabolism on anoikis resistance in a panel of lung cancer cells. Targeting glutaminolysis by glutamine deprivation or glutamine antagonist 6-diazo-5-oxo-L-norleucine (DON) treatment for a short period of time (24 hours) induced significantly more apoptotic cell death when cells were detached than attached in majority of lung cancer cells tested (Figure 1C). Interestingly, the cells that responded to glutaminolysis inhibition in terms of anoikis induction were commonly lacking LKB1. These data suggest that although GDH1 expression is induced upon detachment in all cells regardless of LKB1, glutaminolysis may be critical in protecting cells from anoikis only in lung cancer cells that are lack of LKB1.

Reliance of GDH1 on anoikis resistance depends on LKB1 status

To investigate the effect of LKB1 status on GDH1-mediated anoikis resistance, we generated isogenic pairs of lung cancer cell lines with different LKB1 status. Expression of wild-type (WT) but not a kinase-dead (KD) form of LKB1 in LKB1-deficient cells abolished the effect of GDH1 knockdown on anoikis induction (Figure 1D *upper*). On the contrary, knockout of LKB1 in LKB1 wt cells restored the GDH1 knockdown effect, resulting in enhanced anoikis induction (Figure 1E *upper*). Interestingly, LKB1 removal led to decreased phosphorylation of its downstream effectors AMPK and ACC1, and GDH1 knockdown led to further attenuation of these phosphorylations specifically in cells lacking LKB1 (Figure 1D and 1E *lower*). This observation suggests that GDH1 contributes to anoikis resistance and activation of LKB1 downstream effector AMPK exclusively in the absence of LKB1.

GDH1 confers anoikis resistance and metastatic potential to lung cancer cells

To further demonstrate whether GDH1 is important for anti-anoikis signaling in lung cancer, we assessed the impact of targeting GDH1 on anoikis induction of a panel of NSCLC cells using multiple shRNA clones. GDH1 knockdown sensitized a group of lung cancer cells including A549, H157, and H460 to detachment-induced apoptosis which are LKB1 null, whereas a group of cells that harbor wild-type LKB1, H1299, H292, and H358, did not respond to GDH1 knockdown in terms of anoikis induction (Figure 2A and S2A). And the GDH1 contribution was specific to detachment-induced apoptosis (Figure S2B). Detachment-induced apoptosis in GDH1 knockdown cells was accompanied by a reduction in mitochondrial membrane potential and cytochrome c release (Figures S2C and S2D). Cell permeable α-KG, product of GDH1, restored the enhanced anoikis induction and cytochrome c release in LKB1-deficient GDH1 knockdown cells (Figures 2B, S2E, and S2F). α-KG but not other TCA intermediate metabolites, including succinate, malate, or fumarate, rescued the anoikis induced by GDH1 targeted downregulation (Figure 2C). Cell permeable dimethyl metabolites were treated with concentrations that fully restore corresponding metabolite levels in detached GDH1 knockdown cells (Figure S2G). Moreover, recovery of GDH activity by overexpressing wild type GDH1 but not enzyme-dead mutant GDH1 R443S rescued the anoikis resistant potential in GDH1 knockdown cells (Figure 2D)(Zaganas et al., 2002). Furthermore, restoration of decreased α-KG level by

overexpressing other α-KG producing mitochondrial enzymes such as glutamic-oxaloacetic transaminase 2 (GOT2) again fully rescued anoikis resistance in GDH1 knockdown cells (Figure 2E). These data together suggest that enzymatic activity of GDH1, in particular its product α-KG, contributes to anoikis resistance. We next functionally validated the role of GDH1 in tumor metastasis using a xenograft model of experimental metastasis, in which tumor cells are injected directly into the systemic circulation. Anoikis resistance can be precisely monitored using this model since the number and type of cells introduced into the circulation can be controlled. The mice transplanted with GDH1 knockdown A549 or H460 cells showed reduced metastasis when compared with the control group injected with cells harboring empty vector, suggesting that GDH1 promotes metastatic potential *in vivo* (Figures 2F and 2G).

GDH1 contributes to anoikis resistance by regulating energy balance through the CamKK2-AMPK pathway

To identify the metabolic advantages GDH1 provides to confer anoikis resistance, we performed a series of metabolic assays in lung cancer cells with GDH1 knockdown. Loss of matrix attachment resulted in metabolic impairment limiting the uptake of nutrients and consequently decreasing flux through metabolic pathways including the TCA cycle, and glutamine metabolism was further decreased with the application of GDH1 knockdown (Figure S3A–S3D). Consistent with previous reports, detachment was accompanied by enhanced reductive carboxylation of glutamine, assessed by increased labelling at citrate m+5, whereas glutamine oxidation reflected by the m+4 fraction of citrate was decreased upon detachment (Figure S3E). However, both reductive and oxidative glutamine metabolism were reduced upon loss of GDH1, indicating that GDH1 plays a critical role in glutamine metabolism in all cases. GDH1 knockdown did not influence anabolic biosynthesis under anoikis-induced conditions (Figure S3F). In contrast to normal culture conditions where GDH1 knockdown impaired ROS regulation through GPx1, GDH1 knockdown did not alter intracellular ROS levels under detached culture conditions (Figure S3G), and the anti-oxidants N-acetyl-L-cysteine (NAC) and tiron could not rescue the anoikis resistance lost due to GDH1 knockdown (Figure S3H). Moreover, knockdown of GPx1, the ROS scavenging enzyme controlled by GDH1, did not sensitize cells to anoikis induction (Figure S3I). GDH1 may not predominantly contribute to redox homeostasis in detached cells where altered metabolism such as reductive carboxylation controls ROS through a different mechanism such as IDH1. These data suggest that GDH1 provides metabolic advantages other than redox regulation or anabolic biosynthesis to confer anoikis resistance. Indeed, GDH1 knockdown decreased ATP levels and oxygen consumption rates whereas α-KG restored the effect under detached culture conditions only in LKB1-defiicent cells, suggesting that GDH1 contributes to energy metabolism in LKB1-deficient cancer cells once detached from the extracellular matrix (Figures 3A, S3J–S3L).

To explore the mechanism by which GDH1 contributes to anti-anoikis signaling, we examined whether GDH1 knockdown attenuates the activity of AMPK, a master regulator of cellular energy homeostasis. We found that AMPK activity, assessed by AMPKα T172 phosphorylation, was significantly attenuated in GDH1 knockdown cells compared to control cells, whereas the GDH1 product α-KG but not other intermediate metabolites

rescued the decreased AMPK activation in GDH1 knockdown cells when detached (Figures 3B *left* and S4A). In agreement, rescue of intracellular α-KG either by GDH1 WT or another α-KG producing enzyme, GOT2, reactivated AMPK in GDH1 knockdown cells (Figures 3B *right* and 3C). These results further demonstrate that the GDH1 product α-KG plays a pivotal role in AMPK activation and anoikis resistance. GDH1 knockdown decreased intracellular ATP level and anoikis resistance (Figure 3D and 3E; *left two panels*). Decreased ATP was not rescued by the addition of caspase inhibitor Z-VAD suggesting that the change in ATP production was not a consequence of anoikis, but that impaired energy homeostasis upon GDH1 knockdown leads to anoikis activation (Figure S4B). Restoration of active AMPK by AMPKα overexpression or AMPK activator A769662 significantly rescued the GDH1 knockdown effect on anoikis (Figures 3D and 3E; *right two panels*). Moreover, targeted downregulation of AMPK mimicked the GDH1 knockdown effect in terms of anoikis induction (Figure 3F). In addition, enhanced anoikis and decreased ATP levels in GDH1 knockdown cells were rescued by treatment with the mTOR inhibitor rapamycin (Figure 3G). These data together suggest that GDH1 and its product α-KG potentiate anoikis resistance by triggering energy metabolism through AMPK activation and consequent suppression of mTOR signaling. However, the effect of α-KG on AMPK was indirect, since the activity of AMPK by phosphorylation and dephosphorylation was not altered by various concentrations of α-KG including the physiological range *in vitro* (Figures 3H and S4C).

To investigate how GDH1 contributes to AMPK activation and anoikis resistance in an LKB1 independent manner, we tested the effect of targeting GDH1 on the activities of CamKK2, the known alternative upstream kinases of AMPK. GDH1 knockdown decreased the activity of CamKK2, which was fully rescued by treatment with α-KG (Figure 4A). CamKK2 transient knockout approach revealed that CamKK2 largely governs AMPK activity and anoikis resistance in LKB1-deficient cells, but not in LKB1 wt cells (Figure 4B). To further validate that GDH1 controls anoikis resistance through CamKK2, we tested whether CamKK2 overexpression can reverse the GDH1 knockdown effect. Indeed, overexpression of CamKK2 rescued the decreased AMPK activity and anoikis resistance in GDH1 knockdown cells (Figure 4C). In contrast, treatment of CamKK2 inhibitor STO-609 attenuated AMPK activation and sensitized the cells to anoikis induction, while GDH1 knockdown cells were resistant to the CamKK2 inhibitor (Figure 4D). Moreover, CamKK2 inhibition using BAPTA eradicated the α-KG rescue effect in GDH1 knockdown cells (Figure S5A). These data together suggest that GDH1 and its product α-KG promote anti-anoikis signaling by activating AMPK through CamKK2, and this contribution is pronounced in LKB1-deficient cells where CamKK2 plays a dominant role in activating AMPK.

We next explored the molecular mechanism underlying α-KG mediated activation of CamKK2. Radiometric metabolite-protein interaction assay and cellular thermal shift assay revealed that α-KG specifically binds to CamKK2 (Figures 4E and 4F). Calcium controls the activity of CamKK2. Manipulation of GDH1 and its product α-KG did not alter calcium levels suggesting that GDH1 and α-KG mediated CamKK2 activation does not occur through calcium (Figure S5B). Whereas, treatment with cell permeable α-KG enhanced CamKK2 substrate AMPKα binding to CamKK2 in cells (Figure 4G). Furthermore, α-KG

treatment increased AMPKα binding to CamKK2 in a dose-dependent manner *in vitro* using purified AMPKα-CamKK2-calmodulin complex (Figure 4H). These data suggest that α-KG promotes CamKK2 activity by enhancing CamKK2 binding to its substrate AMPKα.

GDH1 small molecule inhibitor R162 attenuates anoikis resistance and tumor metastasis

Our finding that GDH1 is upregulated in metastatic lung cancer and GDH1 knockdown attenuates anoikis resistance and tumor metastasis implicates GDH1 as an attractive anti-metastasis target. We previously screened and identified purpurin and its cell permeable analog R162 as GDH1 selective inhibitors (Jin et al., 2015). Treatment with R162 significantly sensitized LKB1-deficient A549, H157, and H460 cells to anoikis induction, and this was fully rescued by α-KG treatment (Figures 5A and S6). The dose of 20 mg/kg/day R162 treatment significantly attenuated metastatic potential in a xenograft mouse model injected with luciferase labeled A549 cell lines (Figure 5B). To test the efficacy of GDH1 inhibitor as an anti-metastasis drug in a more clinically relevant setting, we established a patient-derived xenograft (PDX) model using an LKB1-deficient lung cancer patient-derived tumor (Figure 5C). The PDX tumors injected in an experimental metastasis model through the tail vein survived in the circulation and colonized to liver, lungs and other organs, whereas R162 treatment dramatically attenuated their metastatic potential in PDX mice (Figures 5D–5F). These results together suggest that GDH1 is a promising anti-metastasis target and that the GDH1 inhibitor R162 is a potent agent for anti-metastasis therapy in LKB1-deficient human lung cancer.

Transcription factor PLAG1 controls GDH1 expression in lung cancer

To glean comprehensive mechanistic insight into how GDH1 is upregulated in anoikis induced lung cancer cells, we performed transcription factor (TF) activation profiling using attached and detached A549 cells. The TF Activation Profiling Array monitors activities of 96 cellular TFs, including NFκB, HIF1, and p53, that are known to play essential roles in regulating gene expression (Toubal et al., 2013). Five among 96 TFs were activated more than 1.8-fold when cells were cultured under detached conditions, including PLAG1, SATB1, and Snail3 (Figure 6A). To further examine whether any of these TFs activate the GDH1 promoter, we overexpressed the top 3 potential candidates PLAG1, SATB1, and Snail3, and performed a GDH1 promoter reporter activity assay. PLAG1 but not SATB1 or Snail3 enhanced GDH1 promoter activity (Figure 6B). A promoter reporter activity assay using GDH1 and GDH2 promoter reporters revealed that PLAG1 mainly enhances GDH1 promoter activity (Figure 6C). In addition, chromatin immunoprecipitation (ChIP) assay showed that the GDH1 promoter interacts with PLAG1 but not SATB1 in 293T cells and lung cancer A549 cells (Figure 6D). Moreover, knockdown of PLAG1 attenuated GDH1 expression and GDH1 promoter activity, and enhanced apoptosis under detached conditions, suggesting that PLAG1 contributes to GDH1 expression and confers anoikis resistance in lung cancer cells (Figure 6E).

Finally, we clinically validated our functional studies of tumor metastasis using a panel of primary and metastatic paired lung cancer patient tumor tissues. LKB1 status of the 80 paired tumors was determined by LKB1 immunohistochemistry (IHC) staining (Figure 7A). PLAG1 expression significantly correlated with the status of metastasis in both LKB1

negative and positive tumors (Figure 7B). While GDH1 expression levels were higher in metastasized tumors than the paired primary tumors when lacking LKB1, there was no significant difference in the tumor pairs expressing LKB1 (Figure 7C). In line with the correlation between metastatic status and PLAG1 or GDH1 expression, the staining intensity of PLAG1 and GDH1 positively correlated in both LKB1-negative and -positive sets of tumors (Figure 7D). In contrast, a significant positive correlation between GDH1 expression and AMPKα phosphorylation only existed in LKB1-deficient tumors, but not in tumors carrying LKB1 (Figure 7E). Our finding was further clinically validated by analyzing TCGA lung cancer datasets. A positive correlation between GDH1 expression and AMPK activation only exists in lung cancer patients whose tumors lack functional LKB1, but not in patients with tumor carrying wild type LKB1, further supporting that GDH1 contributes to AMPK activation in tumor cells lacking LKB1 (Figure 7F). Our study supports the role of GDH1 signaling as a metastasis-promoting pathway in lung cancer lacking LKB1. Although PLAG1 induces GDH1 regardless of LKB1 status, only LKB1-deficient tumors may benefit from GDH1 expression and acquire metastatic potential by GDH1-mediated activation of CamKK2 and its downstream effector AMPK.

DISCUSSION

The acquisition of anoikis resistance allows tumor cells to survive while they circulate in the bloodstream and is vital to metastatic progression, but the molecular mechanism by which tumor cells develop anoikis resistance remains unclear. Our findings delineate this mechanism by revealing a crosstalk between mitochondrial glutamine metabolism and tumor metastasis. We demonstrate that enhanced expression of GDH1 mediated by a transcription factor PLAG1 following detachment activates CamKK2 and its downstream substrate AMPK, which provides anti-anoikis and pro-metastatic signaling to lung cancer cells. Although GDH1 is commonly induced by PLAG1 upon detachment, GDH1 is critical in LKB1-null cells where GDH1-mediated activation of CamKK2 plays a pivotal role in activating AMPK that contributes to anoikis resistance and tumor metastasis, while GDH1 has less effect in cells with LKB1-wt where AMPK activation is predominantly dependent on LKB1 not the GDH1 signaling effector, CamKK2 (Figure 7G). Therefore, targeting GDH1 would be a promising therapeutic opportunity to prevent the development of metastasis in LKB1-deficient lung cancer.

Our study suggests a differential role of GDH1 in the metabolism of lung cancer cells with different LKB1 status. Our results also reveal that the status of LKB1 differentially reprograms the metabolic requirements in cancer cells for survival during tumor metastasis. We recently reported that GDH1 is important for redox homeostasis by controlling its product α-KG and a subsequent metabolite fumarate, which provides a proliferative advantage for rapidly growing tumors. While GDH1 is commonly important for redox regulation, cancer cell proliferation and tumor growth despite LKB1 status, GDH1 has an additional role in the regulation of bioenergetics in LKB1-null cells upon detachment. Tumor cells may slow down the generation of building blocks or the management of redox balance as a means for bioenergetics conservation during extracellular membrane detachment, and elevated GDH1 may contribute to this response by having an additional role when tumor cells disseminate. However, there are reports implicating the role of redox

regulation in anoikis resistance. Studies demonstrate that ROS is deleterious and must be neutralized by antioxidant enzymes in detached breast cancer cells (Avivar-Valderas et al., 2011; Davison et al., 2013; Schafer et al., 2009). Conversely, hydrogen peroxide is reported as an anti-anoikis promoting factor by stabilizing the metastasis gene caveolin-1 in lung cancer (Rungtabnapa et al., 2011). This implies that the metabolic demand for detached tumor cells may differ depending on cancer type and disparate metabolic conditions such as antioxidant enzyme activities.

We found that mechanistically, the GDH1 product α-KG activates CamKK2 by enhancing the binding of its substrate AMPK to CamKK2. This provides additional evidence that metabolic intermediates function as signaling molecules to allow crosstalk between metabolic pathways and cell signaling pathways. Detailed future study is warranted to decipher by which mechanism α-KG structurally recruits the substrate AMPK to CamKK2. AMPK has recently been implicated in anoikis resistance and is activated either by LKB1 or CamKK2 under detachment-induced stress (Sundararaman et al., 2016). Enhanced AMPK is known to contribute to sustaining pro-survival signals after detachment by activating an autophagic pathway through Ulk1 phosphorylation and inhibiting mTOR through suppressing energy-demanding protein synthesis (Avivar-Valderas et al., 2013; Kim et al., 2011; Ng et al., 2012). In addition, AMPK contributes to anoikis resistance in breast cancer by phosphorylating PEA15 at serine 16 (Hindupur et al., 2014). We showed that GDH1-mediated activation of AMPK contributes to anoikis resistance through mTOR inhibition in LKB1-deficient lung cancer.

We identified PLAG1 as a transcription factor for GDH1. Although detachment commonly enhanced GDH1 expression, only LKB1-deficient cells benefit from enhanced GDH1 expression by α-KG-mediated CamKK2 activation. Moreover, our findings that GDH1 expression positively correlates with lung cancer metastatic progression and GDH1 knockdown not only reduces tumor growth, but also sensitizes cells to anoikis induction and attenuates tumor metastasis, suggest that GDH1 may represent an attractive anti-cancer and anti-metastasis target for the treatment of lung cancer depending on the LKB1 status. Compound R162, as a first generation of GDH1 small molecule inhibitor for GDH1-targeted lung cancer therapy, has shown promising efficacy in the treatment of lung cancer cells and in PDX mouse models of tumor metastasis. The strategy of targeting GDH1 has the potential to be commonly effective for all lung cancer patients with elevated glutamine metabolism, and more beneficial to those patients who are diagnosed with LKB1-deficient metastatic lung cancer, for which there is currently a lack of effective inhibitor.

STAR METHODS

Detailed methods are provided in the online version of this paper and include the following:

KEY RESOURCES TABLE

REAGENT or RESOURCE	SOURCE	IDENTIFIER
Antibodies		

REAGENT or RESOURCE	SOURCE	IDENTIFIER
Rabbit polyclonal anti-GDH antibody	Abcam	Cat#ab89967; RRID: AB_2263346
Mouse monoclonal anti-beta-actin (clone AC-74) antibody	Sigma-Aldrich	Cat#A2228; RRID: AB_476697
Mouse monoclonal anti-cytochrome C (clone 7H8.2C12) antibody	BD Biosciences	Cat#556433; RRID: AB_396417
Mouse monoclonal anti-alpha-tubulin (clone B-7) antibody	Santa Cruz Biotechnology	Cat#sc-5286; RRID: AB_628411
Rabbit monoclonal anti-Cox IV (clone 3E11) antibody	Cell Signaling Technology	Cat#4850; RRID: AB_2085424
Rabbit polyclonal anti-GFP antibody	Santa Cruz Biotechnology	Cat#sc-8334; RRID: AB_641123
Rabbit monoclonal anti-GPx1 (clone EPR3311) antibody	Abcam	Cat#ab108429; RRID: AB_10865045
Rabbit monoclonal anti-AMPK-alpha phospho (Thr172) (clone 40H9) antibody	Cell Signaling Technology	Cat#2535; RRID: AB_331250
Rabbit monoclonal anti-AMPK alpha (clone D5A2) antibody	Cell Signaling Technology	Cat#5831; RRID: AB_10622186
Rabbit monoclonal anti-phospho-ACC1 (S79) (clone D7D11) antibody	Cell Signaling Technology	Cat#11818; RRID: AB_2687505
Rabbit monoclonal anti-ACC1 (clone C83B10) antibody	Cell Signaling Technology	Cat#3676; RRID: AB_2219397
Rabbit monoclonal anti-LKB1 (clone D60C5) antibody	Cell Signaling Technology	Cat#3047; RRID: AB_2198327
Mouse monoclonal anti-FLAG (clone M2) antibody	Sigma-Aldrich	Cat#F3165; RRID: AB_259529
Rabbit polyclonal anti-CamKK2 (clone H-95) antibody	Santa Cruz Biotechnology	Cat#sc-50341; RRID: AB_2068532
Mouse monoclonal anti-calmodulin antibody	Millipore	Cat#05-173; RRID: AB_309644
Mouse monoclonal anti-V5 probe (clone E10) antibody	Santa Cruz Biotechnology	Cat#sc-81594; RRID: AB_1131162
Rabbit polyclonal anti-PLAG1 antibody	Novus Biologicals	Cat#NBP2-15075
Rabbit monoclonal anti-SATB1 (clone EPR3895) antibody	Abcam	Cat#ab92307; RRID: AB_2050287
Mouse monoclonal anti-PLAG1 antibody (clone 3B7) for IHC	Enzo Life Sciences	Cat#H00005324-M02; RRID: AB_1506877
Rabbit monoclonal anti-LKB1 antibody (D60C5F10) for IHC	Cell Signaling Technology	Cat#13031
Biological Samples		
Human lung tumor tissues	US Biomax	Cat#LC814 and LC817
Patient-derived xenografts (PDX)	Owonikoko et al., 2016	N/A
Chemicals, Peptides, and Recombinant Proteins		
6-diazo-5-oxo-L-norleucine (DON)	Sigma-Aldrich	Cat#D2141; CAS: 157-03-0
Rapamycin	Sigma-Aldrich	Cat#R0395; CAS: 53123-88-9
Cycloheximide	Sigma-Aldrich	Cat#C4859; CAS: 66-81-9
Taxol	Sigma-Aldrich	Cat#T7191; CAS: 33069-62-4
Actinomycin D	Sigma-Aldrich	Cat#A1410; CAS: 50-76-0

REAGENT or RESOURCE	SOURCE	IDENTIFIER
Etoposide	Selleckchem	Cat#S1225; CAS: 33419-42-0
Dimethyl-alpha ketoglutarate	Sigma-Aldrich	Cat#75890; CAS: 13192-04-6
Dimethyl fumarate	Sigma-Aldrich	Cat#242926; CAS: 624-49-7
Dimethyl succinate	Sigma-Aldrich	Cat#W239607; CAS: 106-65-0
Dimethyl L-malate	Sigma-Aldrich	Cat#374318; CAS: 617-55-0
alpha ketoglutaric acid	Sigma-Aldrich	Cat#349631; CAS: 328-50-7
NAC	Sigma-Aldrich	Cat#A7250; CAS: 616-91-1
Tiron	Sigma-Aldrich	Cat#172553; CAS: 270573-71-2
A769662	LC Laboratories	Cat#A-1803; CAS: 844499-71-4
STO-609	Calbiochem	Cat#570250; CAS: 52029-86-4
BAPTA, AM	Invitrogen	Cat#B1205
CM-H2DCFDA	Invitrogen	Cat#C6827
Fluo-3, AM	Invitrogen	Cat#F1242
Fura Red, AM	Invitrogen	Cat#F3021
R162	Sigma-Aldrich	Cat#R162205; CAS: 64302-87-0
D-[U-^{14}C] glucose	Perkin Elmer	Cat#NEC042X050UC
L-[U-^{14}C] glutamine	Perkin Elmer	Cat#NEC451050UC
α-[1-^{14}C] Ketoglutaric Acid	Perkin Elmer	Cat#NEC597050UC
[1,4-^{14}C] Fumaric acid	Moravek	Cat#MC 2509
L-[U-^{13}C] glutamine	Cambridge Isotope Laboratories	Cat#CLM-1822-H-PK
D-Luciferin	Perkin Elmer	Cat#122799
AMPK A1/B1/G1	SignalChem	Cat#P47-10H
CamKK2	SignalChem	Cat#C18-10G
Calmodulin	SignalChem	Cat#C02-39B-500
PP2Calpha	SignalChem	Cat#P02-20G
AMPK alpha	Abnova	Cat#H00005562-Q01
SAMStide	SignalChem	Cat#S07-58
Dialyzed Fetal Bovine Serum	Sigma-Aldrich	F0392
Critical Commercial Assays		
FITC Annexin V Apoptosis Detection Kit	BD Biosciences	Cat#556547
Caspase-Glo 3/7 assay	Promega	Cat#G8090
Chromatin Immunoprecipitation (ChIP) Assay	Millipore	Cat#17-295
MitoProbe JC-1 Assay Kit	Invitrogen	Cat#M34152
Alpha-ketoglutarate Assay	Abcam	Cat#ab83431
ATP Bioluminescent Assay Kit	Sigma	Cat#FLAA
Malate Assay	Abcam	Cat#ab83319
Succinate Assay	Abcam	Cat#ab204718

REAGENT or RESOURCE	SOURCE	IDENTIFIER
Ammonia Assay	Abcam	Cat#ab83360
Fumarate Assay	Abcam	Cat#ab102516
Glutamine/Glutamate-Glo Assay	Promega	Cat#J8021
Glucose-Glo Assay	Promega	Cat#J6021
Lactate-Glo Assay	Promega	Cat#J5021
TF Activation Profiling Plate Array II	Signosis	Cat#FA-1002
Mitochondria Isolation Kit	Thermo Scientific	Cat#89874
Experimental Models: Cell Lines		
Human: A549 cells	ATCC	Cat#CCL-185
Human: H157 cells	ATCC	Cat#CRL-5802
Human: H460 cells	ATCC	Cat#HTB-177
Human: H1299 cells	ATCC	Cat#CRL-5803
Human: H292 cells	ATCC	Cat#CRL-1848
Human: H358 cells	ATCC	Cat#CRL-5807
Experimental Models: Organisms/Strains		
Mouse: Hsd:Athymic Nude-Foxn1nu	Envigo	Cat#069
Mouse: NOD.Cg-*Prkdc*^{scid} *Il2rg*^{tm1Wjl}/SzJ	The Jackson Laboratory	Cat#JAX:005557; RRID: IMSR_JAX:005557
Oligonucleotides		
shRNA targeting sequence: GDH1 #1: GCCATTGAGAAAGTCTTCAAA	Dharmacon	Cat#TRCN0000028600
shRNA targeting sequence: GDH1 #2: CCCAAGAACTATACTGATAAT	Dharmacon	Cat#TRCN0000028588
shRNA targeting sequence: GPx1 #1: GCAAGGTACTACTTATCGAGA	Dharmacon	Cat#TRCN0000046228
shRNA targeting sequence: GPx1 #2: CTTCGAGAAGTGCGAGGTGAA	Dharmacon	Cat#TRCN0000046230
shRNA targeting sequence: AMPK alpha #1: GCATAATAAGTCACAGCCAAA	Dharmacon	Cat#TRCN0000000857
shRNA targeting sequence: AMPK alpha #2: CCATCCTGAAAGAGTACCATT	Dharmacon	Cat#TRCN0000000858
shRNA targeting sequence: PLAG1 #1: CCAGCAGTTTAAGCACAAGTA	Dharmacon	Cat#TRCN0000020545
shRNA targeting sequence: PLAG1 #2: CCACCAAATGATCACAACTTT	Dharmacon	Cat#TRCN0000020548
sgRNA targeting sequence: LKB1 #1: CTTCAAGGTGGACATCTGGT	This paper	N/A
sgRNA targeting sequence: LKB1 #2: GAGGGCGAGCTGATGTCGGT	GeneCopoeia	Cat#HCP217794-LvSG03-1-B
sgRNA targeting sequence: CamKK2 #1: CAGCAACCGGGCCGCCCCCC	GeneCopoeia	Cat#HCP200782-LvSG03-3-B-a
sgRNA targeting sequence: CamKK2 #2: ACACTCGGTGACCACAATGA	GeneCopoeia	Cat#HCP200782-LvSG03-3-B-b
Primer: ChIP for GDH1 Forward AGAGGACAGGCCAGGGTGGGC	This paper	N/A

REAGENT or RESOURCE	SOURCE	IDENTIFIER
Primer: ChIP for GDH1 Reverse GCGTGGGTGAGGCTTGGCGGT	This paper	N/A
Primer: GLUL Forward AAGAGTTGCCTGAGTGGAATTTC	This paper	N/A
Primer: GLUL Reverse AGCTTGTTAGGGTCCTTACGG	This paper	N/A
Primer: SLC1A5 Forward GAGCTGCTTATCCGCTTCTT	This paper	N/A
Primer: SLC1A5 Reverse GGGGCGTACCACATGATCC	This paper	N/A
Primer: SLC7A5 Forward CCGTGAACTGCTACAGCGT	This paper	N/A
Primer: SLC7A5 Reverse CTTCCCGATCTGGACGAAGC	This paper	N/A
Primer: GLS1 Forward AGGGTCTGTTACCTAGCTTGG	This paper	N/A
Primer: GLS1 Reverse ACGTTCGCAATCCTGTAGATTT	This paper	N/A
Primer: GLS2 Forward GCCTGGGTGATTTGCTCTTTT	This paper	N/A
Primer: GLS2 Reverse CCTTTAGTGCAGTGGTGAACTT	This paper	N/A
Primer: GDH1/2 Forward AGTTCCAAGACAGGATATCGGG	This paper	N/A
Primer: GDH1/2 Reverse TCAGGTCCAATCCCAGGT	This paper	N/A
Primer: GDH1/2 Forward CCGTGGTGTCTTCCATGGGATTG	This paper	N/A
Primer: GDH1/2 Reverse GCAAGTGGTAGTTAGAATCCC	This paper	N/A
Primer: GPT1 Forward GGGTTCGCAGTTCCACTCATT	This paper	N/A
Primer: GPT1 Reverse CCGCACACTCATCAGCTTCA	This paper	N/A
Primer: GPT2 Forward GTGATGGCACTATGCACCTAC	This paper	N/A
Primer: GPT2 Reverse TTCACGGATGCAGTTGACACC	This paper	N/A
Primer: GOT1 Forward ATGGCACCTCCGTCAGTCT	This paper	N/A
Primer: GOT1 Reverse AGTCATCCGTGCGATATGCTC	This paper	N/A
Primer: GOT2 Forward AGCCTTACGTTCTGCCTAGC	This paper	N/A
Primer: GOT2 Reverse AAACCGGCCACTCTTCAAGAC	This paper	N/A
Primer: PLAG1 Forward ATCACCTCCATACACACGACC	This paper	N/A
Primer: PLAG1 Reverse AGCTTGGTATTGTAGTTCTTGCC	This paper	N/A

REAGENT or RESOURCE	SOURCE	IDENTIFIER
Primer: GAPDH Forward GACATCAAGAAGGTGGTG	This paper	N/A
Primer: GAPDH Reverse GTCATACCAGGAAATGAGC	This paper	N/A
Recombinant DNA		
Plasmid: pLHCX	Clonetech	Cat#S1866
Plasmid: Gateway pDEST27	Invitrogen	Cat#11812013
Plasmid: pLHCX-Gateway	This paper	N/A
Plasmid: pLHCX-flag-AMPK alpha2	This paper	N/A
Plasmid: pLHCX-flag-CamKK2	This paper	N/A
Plasmid: MGC Human GDH1 Sequence-Verified cDNA	Dharmacon	MHS6278-202759569
Plasmid: MGC Human GDH2 Sequence-Verified cDNA	Dharmacon	MHS6278-202759832
Plasmid: pLHCX-GDH1	This paper	N/A
Plasmid: pLHCX-GDH1 R443S	This paper	N/A
Plasmid: pDEST27-CamKK2	This paper	N/A
Plasmid: pcDNA3-LKB1 WT	Addgene	Cat#8590
Plasmid: pcDNA3-LKB1 K78I	Addgene	Cat#8591
Plasmid: pLNES-HSV1-tk/GFP-cmvFLuc	Kang et al. 2005	N/A
Plasmid: pLentiCRISPR v2	Addgene	Cat#52961
Plasmid: pLX304/V5-SATB1	DNASU	Cat#HsCD00435476
Plasmid: pLX304/V5-Snail3	DNASU	Cat#HsCD00436805
Plasmid: pLX304/V5-GPT2	Dharmacon	Cat#OHS6085-213576999
Plasmid: pLX304/V5-GOT2	DNASU	Cat#HsCD00438253
Plasmid: pLX304/V5-IDH2	DNASU	Cat#HsCD00438305
Plasmid: pLHCX-flag-PLAG1	This paper	N/A
Plasmid: LightSwtich GLUD1 Promoter Reporter	SwitchGear Genomics	Cat#S711017
Plasmid: LightSwtich GLUD2 Promoter Reporter	SwitchGear Genomics	Cat#S701638
Deposited Data		
Original images were deposited to Mendeley data	This paper	http://dx.doi.org/10.17632/r23kcs7s8n.1
Software and Algorithms		
GraphPad Prism 7 software	GraphPad Software	http://www.graphpad.com
GDH1 mRNA and AMPK T172p expression z-scores	cBioportal	http://www.cbioportal.org
LKB1 mutational status of lung cancer patients	Firehose	http://gdac.broadinstitute.org/

CONTACT FOR REAGENT AND RESEOURCE SHARING

Further information and requests for resources and reagents should be directed to and will be fulfilled by the Lead Contact, Sumin Kang (smkang@emory.edu).

EXPERIMENTAL MODEL AND SUBJECT DETAILS

Cell culture—Lung cancer cells were cultured in RPMI 1640 medium with 10% FBS. 293T cells were cultured in DMEM with 10% FBS.

Animal studies—Animal experiments were performed according to protocols approved by the Institutional Animal Care and Use Committee of Emory University. Nude mice (athymic nu/nu, female, 4–6-week old, Jackson Laboratory) or NSG mice (NOD scid gamma, female, 4–6-week old, Jackson Laboratory) were used for xenograft experiments.

Human studies—Approval to use human specimens was given by the Institutional Review Board of Emory University. All clinical samples were collected with informed consent under Health Insurance Portability and Accountability Act (HIPAA) approved protocols. Paraffin-embedded lung cancer patient tumors were obtained from US Biomax (LC814 and LC817).

Cell lines—A549, H157, H460, H1299, H292, and H358 cell lines were cultured in RPMI 1640 medium with 10% fetal bovine serum (FBS). 293T cells were cultured in Dulbecco Modified Eagle Medium (DMEM) with 10% FBS.

METHOD DETAILS

Lentivirus and retrovirus production, RNAi and protein overexpression in human cancer cells—To knockdown endogenous human GDH1, AMPKα, and PLAG1, lentivirus carrying shRNA were generated by transfecting 293T cells with lentiviral vector encoding shRNA, psPAX2, and pMD2.G. Cells were infected with harvested lentivirus for 48 hours for transient infection or were selected by 2 μg/ml puromycin for stable selection. For LKB1 and CamKK2 knockout, pCRISPR-SG01 or plentiCRISPR v2 vectors encoding LKB1 or CamKK2 sgRNA were transiently transfected into lung cancer cells using Lipofectamine 3000 (Invitrogen). AMPK, LKB1, or CamKK2 were overexpressed in human cancer cells using retroviral vectors pLHCX-Gateway encoding target genes. Selection was carried out for 7–10 days with 300 μg/ml hygromycin for stable expression.

Anoikis assay—Cells were cultured on 1% agar treated plate for 48 h. Apoptotic cell death induced by detachment was determined by using Caspase-Glo 3/7 Assay (Promega) for Figure 2A *bottom*, and Annexin V Apoptosis Detection Kit (BD Pharmingen) for others based on the manufactures' protocol.

Quantitative RT-PCR—RNA was isolated using RNeasy kit (Qiagen). qRT-PCR was conducted with High-Capacity cDNA Reverse Transcription Kit (Applied Biosystems) and iTaq™ Universal SYBR Green Supermix (Bio-Rad). Primers were designed using PrimerBank (Spandidos et al., 2010). The sequences of primers are listed in Key Resource Table.

Metabolic assays—Intracellular ATP concentration and ATP/ADP ratio were determined using ATP bioluminescent somatic cell assay (Sigma) and ADP/ATP Ratio Assay Kit (Abcam), respectively. Intracellular α-KG, succinate, fumarate and malate levels were assessed using commercial assay kits from Abcam. Briefly, 2×10^6 cells for each group

were collected and the cell volume was estimated by comparing the size of the cell pellet with the size of known-volume PBS in a separate tube. Cell pellets were homogenized with assay buffer and the debris was removed by centrifugation. The supernatant was further deproteinized using Amicon Ultra-10k centrifugal filter (Millipore) and subjected to metabolites measurement according to the manufacturer's recommendation. Glucose consumption, lactate production and glutamine consumption were determined using commercial kits from Promega. Briefly, culture medium from cells cultured in attached or detached condition were collected at different timepoints and used for measurement of glucose, lactate and glutamine. Ammonia release in the cell culture medium was determined using Ammonia Assay Kit (Abcam). Oxygen consumption rate was measured using a clark-type oxygen sensor (Strathkelvin Instruments). For basal and maximum OCR, cells were sequentially treated with oligomycin (500 nM), FCCP (500 nM), and rotenone/antimycin A (1 μM) and analyzed using Seahorse XF24 analyzer (Agilent Technologies). For ^{14}C-RNA and ^{14}C-lipid syntheses, cells were spiked with 4 μCi/ml of D-[U-^{14}C] glucose or L-[U-^{14}C] glutamine (Perkin Elmer) for 2 hours. Extracted ^{14}C-RNA was quantified by liquid scintillation counting and normalized by the total amount of RNA. Lipids were extracted by 500 μL of hexane:isopropanol (3:2 v/v), air dried, suspended in 50 μL of chloroform, and subjected to scintillation counting. For glutaminolysis rate assay, glutamine oxidation measuring $^{14}CO_2$ from ^{14}C glutamine was used to determine glutaminolysis rate. Briefly, cells were seeded under attached or detached condition in 6-cm dishes that were placed in a sealed 10-cm dish. After 24 h, cells were incubated with 4 μCi/ml of [U-^{14}C] glutamine for 4 h and the reaction was stopped by the addition of 200 μl of 70% perchloric acid. 0.5 ml of 3 M NaOH was injected to a cup placed next to the 6-cm dish to absorb all the released CO_2 from the cells. After 12 h incubation, 20 μl of NaOH was subjected to liquid scintillation counting. Cellular ROS was determined with carboxy-H_2DCFDA (Invitrogen). Mitochondria membrane potential was determined using MitoProbe JC-1 Assay Kit (ThermoFisher). Intracellular calcium level was determined by ratiometric analysis of Fura Red (Invitrogen) and Fluo-3 (Invitrogen) staining using flow cytometry, according to manufacturer's instruction.

Metabolite extraction, GC-MS, and ^{13}C metabolic flux analysis—2×10^6 A549 cells without or with GDH1 shRNA were cultured under attached or detached conditions for 24 hours in glutamine-free RPMI-1640 medium containing 2 mmol/L [U-$^{13}C_5$] glutamine and 10% dialyzed FBS. Cells were rinsed with 0.9% saline solution and lysed with 500 μL ice-cold methanol for 1 min. 200 μL water containing 5μg/ml norvaline was added and vortexed. 500μL chloroform was added and vortexed again. After centrifugation at 13,000 rpm for 5 min, 500μL of the upper aqueous layer was collected and evaporated under vacuum at −4°C. Dried polar metabolites were processed for gas chromatography (GC) mass spectrometry (MS). Briefly, polar metabolites were derivatized using a Gerstel MultiPurpose Sampler. Methoxime-tBDMS derivatives were formed by addition of 15 μL 2% (w/v) methoxylamine hydrochloride (MP Biomedicals) in pyridine and incubated at 45°C for 60 min. Samples were silylated by addition of 15 μL of N-tert-butyldimethylsily-Nmethyltrifluoroacetamide (MTBSTFA) with 1% tert-butyldimethylchlorosilane (tBDMS) (Regis Technologies) and incubated at 45°C for 30 min. Derivatized samples were injected into a GC-MS using a DB-35MS column (Agilent J&W Scientific) installed in an Agilent

7890B GC system integrated with an Agilent 5977a MS. Samples were injected at a GC oven temperature of 100°C and held for 1 min before ramping to 255°C at 3.5°C/min then to 320°C at 15°C/min. Electron impact ionization was performed with the MS scanning over the range of 100–650 m/z for polar metabolites. Metabolite levels and mass isotopomer distributions of derivatized fragments were analyzed with an in house Matlab script, which integrated the metabolite fragment ions and corrected for natural isotope abundances.

***In vitro* kinase assays and phosphatase assay—**For CamKK2 *in vitro* kinase assay, endogenous CamKK2 was immunoprecipitated by CamKK2 antibody and applied to kinase assays (40 mM Tris [pH 7.5], 20 mM $MgCl_2$, 200 μM ATP, and 0.1 mg/ml BSA) using recombinant AMPKα as a substrate. The activity of CamKK2 was determined by either ADP-Glo Assay (Promega) or phospho-AMPKα (Thr172) western blot. *In vitro* AMPK kinase assay and PP2c phosphatase assay were performed using SAMStide and recombinant AMPKαβγ complex.

Radiometric metabolite-protein binding assay and cellular thermal shift assay —GST or flag tagged CamKK2 or AMPKα was purified from 293T cells. Bead-bound CamKK2 or AMPKα was incubated with 0.12 μCi of ^{14}C-α-KG or ^{14}C-fumarate for 30 min, washed, eluted, and radioactivity was detected by scintillation counting. Cellular thermal shift assay was performed as previously described (Gad et al., 2014; Martinez Molina et al., 2013). In brief, 293T cells were transfected with flag-CamKK2 and treated with PBS, methyl-α-KG, or methyl-fumarate for 24 h. Cells were collected, aliquoted, and heated at 46, 49, 52, 55, 58, 61, 64, 67, and 70°C for 3 min. CamKK2 in the soluble fraction was quantified by FLAG immunoblot.

Transcription factor activity profiling—A549 cells were subjected to attached or detached conditions for 24 h, followed by nuclear protein extraction. The activities of 96 transcription factors were determined by TF Activation Profiling Plate Array (FA-1002, Signosis) according to the manufacturer's protocol.

Promoter reporter assay and ChIP assay—For GDH1 and GDH2 promoter report assay, PLAG1, SATB1, or Snail3 constructs were co-transfected with GDH promoter constructs, and dual luciferase reporter assay (Promega) was carried out according to the manufacturer's instruction. ChIP assay was performed using Millipore chromatin immunoprecipitation assay (Millipore). Briefly, flag-PLAG1 or V5-SATB1 was pulled down from transfected 293T cells. DNA was isolated from the immunoprecipitates and the GDH1 promoter region was amplified by PCR.

Xenograft studies—Nude mice or NOD SCID gamma (NSG) mice were intravenously injected with 2.5×10^6 of A549-luc-GFP or 2×10^6 of H460 cells, respectively. Bioluminescent imaging (BLI) vector were introduced into A549 cells for BLI (Kang et al., 2005; Ponomarev et al., 2004). Metastasis was monitored by bioluminescence imaging (BLI) analysis as previously described (Alesi et al., 2016). In brief, D-luciferin (75 mg/kg) was intraperitoneally administered and images were acquired using IVIS Imaging System (Perkin Elmer). For experimental lung patient-derived xenograft (PDX) metastasis model, fresh tumor (TKO-008) from LKB1-deficient small cell lung carcinoma PDX mice were

digested with tissue dissociation buffer (0.1% collagenase, 0.01% hyaluronidase, 0.01% DNase I in HBSS) for 1 h at 37°C (Owonikoko et al., 2016; Petit et al., 2013). The tumor cells were washed through a strainer with HBSS and counted. 2×10^6 live patient-derived tumor cells were injected into nude mice through the tail vein. For the R162 efficacy experiment, mice were intraperitoneally injected with vehicle control or R162 (20 mg/kg/day), from the next day of xenograft injection.

Immunohistochemical staining—Paraffin-embedded lung cancer tissue microarrays (LC814 and LC817) containing primary and matched metastasized tumors from lymph nodes were obtained from US Biomax. IHC analyses were performed according to the previously described (Kang et al., 2010). In brief, human tissue sections were deparaffinized, rehydrated, and incubated in 3% hydrogen peroxide to suppress endogenous peroxidase activity. Antigen retrieval was achieved by microwaving the sections in 10 mM Sodium Citrate (pH 6.0). Sections were incubation in 2.5% horse serum for blocking. The primary antibodies were applied to the slides at dilution of 1:250 (anti-LKB1 antibody), 1:200 (anti-PLAG1 antibody), 1:500 (anti-GDH1 antibody), and 1:100 (anti-p-AMPK T172 antibody) at 4°C overnight. Detection was achieved with the avidin–biotin complex system (Vector Laboratories). Slides were stained with 3,3′-diaminobenzidine, washed, counterstained with hematoxylin, dehydrated, treated with xylene, and mounted. Positive staining was identified using IHC signal intensity scored as 0, +1, +2, and +3.

Publicly available TCGA database analysis—GDH1 mRNA expression z-scores (RNA Seq V2 RSEM) and AMPKα T172p protein expression z-scores(RPPA) in TCGA Lung Adenocarcinoma (LUAD) Provisional were downloaded from cBioportal. LKB1 mutation status data from whole exome sequencing was acquired from Firehose. All data were downloaded on 09/01/2016 and Pearson correlation analysis was performed using Graphpad Prism 7.

QUANTIFICATION AND STATISTICAL ANALYSIS

Statistical parameters including the statistical tests used, exact value of n, dispersion and precision measures and statistical significance are reported in the figures and figure legends. Data shown are from one representative experiment of multiple experiments. Statistical analysis of significance was based on chi-square test for Figures 5D, 7D, and 7E, and two-tailed Student's *t* test for all other figures. Data with error bars represent mean ± SD, except for Figures 2F and 2G which show SEM. No statistical method was used to predetermine sample size. For animal studies, animals were randomly chosen and concealed allocation and blinding of outcome assessment was used. For *in vitro* studies, the experiments were not randomized and investigators were not blinded to allocation during experiments and outcome assessment. Statistical analysis and graphical presentation was performed using GraphPad Prism 7.0.

DATA AND SOFTWARE AVAILABILITY

All software used in this study is listed in the Key Resource Table. Original imaging data have been deposited to Mendeley Data and are available at http://dx.doi.org/10.17632/r23kcs7s8n.1.

Supplementary Material

Refer to Web version on PubMed Central for supplementary material.

Acknowledgments

We acknowledge Dr. Anthea Hammond for editorial assistance. This work was supported in part by NIH grants R01 CA175316 (S.K.), R01 CA207768 (S.K.), R01 CA188652 (C.M.), DoD W81XWH-17-1-0186 (S.K.), and Developmental Funds from the Winship Cancer Institute of Emory University (S.K.). F.R.K., and S.K. are Georgia Cancer Coalition Scholars. S. K is a Robbins Scholar and an American Cancer Society Basic Research Scholar.

References

Alesi GN, Jin L, Li D, Magliocca KR, Kang Y, Chen ZG, Shin DM, Khuri FR, Kang S. RSK2 signals through stathmin to promote microtubule dynamics and tumor metastasis. Oncogene. 2016; 35:5412–5421. [PubMed: 27041561]

Avivar-Valderas A, Bobrovnikova-Marjon E, Alan Diehl J, Bardeesy N, Debnath J, Aguirre-Ghiso JA. Regulation of autophagy during ECM detachment is linked to a selective inhibition of mTORC1 by PERK. Oncogene. 2013; 32:4932–4940. [PubMed: 23160380]

Avivar-Valderas A, Salas E, Bobrovnikova-Marjon E, Diehl JA, Nagi C, Debnath J, Aguirre-Ghiso JA. PERK integrates autophagy and oxidative stress responses to promote survival during extracellular matrix detachment. Molecular and cellular biology. 2011; 31:3616–3629. [PubMed: 21709020]

Davison CA, Durbin SM, Thau MR, Zellmer VR, Chapman SE, Diener J, Wathen C, Leevy WM, Schafer ZT. Antioxidant enzymes mediate survival of breast cancer cells deprived of extracellular matrix. Cancer research. 2013; 73:3704–3715. [PubMed: 23771908]

Dela Cruz CS, Tanoue LT, Matthay RA. Lung cancer: epidemiology, etiology, and prevention. Clin Chest Med. 2011; 32:605–644. [PubMed: 22054876]

Faubert B, Vincent EE, Poffenberger MC, Jones RG. The AMP-activated protein kinase (AMPK) and cancer: many faces of a metabolic regulator. Cancer letters. 2015; 356:165–170. [PubMed: 24486219]

Fidler IJ. The pathogenesis of cancer metastasis: the 'seed and soil' hypothesis revisited. Nature reviews. Cancer. 2003; 3:453–458. [PubMed: 12778135]

Gad H, Koolmeister T, Jemth AS, Eshtad S, Jacques SA, Strom CE, Svensson LM, Schultz N, Lundback T, Einarsdottir BO, et al. MTH1 inhibition eradicates cancer by preventing sanitation of the dNTP pool. Nature. 2014; 508:215–221. [PubMed: 24695224]

Grassian AR, Metallo CM, Coloff JL, Stephanopoulos G, Brugge JS. Erk regulation of pyruvate dehydrogenase flux through PDK4 modulates cell proliferation. Genes Dev. 2011; 25:1716–1733. [PubMed: 21852536]

Gupta GP, Massague J. Cancer metastasis: building a framework. Cell. 2006; 127:679–695. [PubMed: 17110329]

Hardie DG, Ross FA, Hawley SA. AMPK: a nutrient and energy sensor that maintains energy homeostasis. Nature reviews. Molecular cell biology. 2012; 13:251–262. [PubMed: 22436748]

Hawley SA, Boudeau J, Reid JL, Mustard KJ, Udd L, Makela TP, Alessi DR, Hardie DG. Complexes between the LKB1 tumor suppressor, STRAD alpha/beta and MO25 alpha/beta are upstream kinases in the AMP-activated protein kinase cascade. J Biol. 2003; 2:28. [PubMed: 14511394]

Hindupur SK, Balaji SA, Saxena M, Pandey S, Sravan GS, Heda N, Kumar MV, Mukherjee G, Dey D, Rangarajan A. Identification of a novel AMPK-PEA15 axis in the anoikis-resistant growth of mammary cells. Breast Cancer Res. 2014; 16:420. [PubMed: 25096718]

Hitosugi T, Fan J, Chung TW, Lythgoe K, Wang X, Xie J, Ge Q, Gu TL, Polakiewicz RD, Roesel JL, et al. Tyrosine phosphorylation of mitochondrial pyruvate dehydrogenase kinase 1 is important for cancer metabolism. Mol Cell. 2011; 44:864–877. [PubMed: 22195962]

Hsu PP, Sabatini DM. Cancer cell metabolism: Warburg and beyond. Cell. 2008; 134:703–707. [PubMed: 18775299]

Jiang L, Shestov AA, Swain P, Yang C, Parker SJ, Wang QA, Terada LS, Adams ND, McCabe MT, Pietrak B, et al. Reductive carboxylation supports redox homeostasis during anchorage-independent growth. Nature. 2016; 532:255–258. [PubMed: 27049945]

Jin L, Alesi GN, Kang S. Glutaminolysis as a target for cancer therapy. Oncogene. 2016; 35:3619–3625. [PubMed: 26592449]

Jin L, Li D, Alesi GN, Fan J, Kang HB, Lu Z, Boggon TJ, Jin P, Yi H, Wright ER, et al. Glutamate dehydrogenase 1 signals through antioxidant glutathione peroxidase 1 to regulate redox homeostasis and tumor growth. Cancer cell. 2015; 27:257–270. [PubMed: 25670081]

Kamarajugadda S, Stemboroski L, Cai Q, Simpson NE, Nayak S, Tan M, Lu J. Glucose oxidation modulates anoikis and tumor metastasis. Molecular and cellular biology. 2012; 32:1893–1907. [PubMed: 22431524]

Kang S, Elf S, Lythgoe K, Hitosugi T, Taunton J, Zhou W, Xiong L, Wang D, Muller S, Fan S, et al. p90 ribosomal S6 kinase 2 promotes invasion and metastasis of human head and neck squamous cell carcinoma cells. The Journal of clinical investigation. 2010; 120:1165–1177. [PubMed: 20234090]

Kang Y, He W, Tulley S, Gupta GP, Serganova I, Chen CR, Manova-Todorova K, Blasberg R, Gerald WL, Massague J. Breast cancer bone metastasis mediated by the Smad tumor suppressor pathway. Proceedings of the National Academy of Sciences of the United States of America. 2005; 102:13909–13914. [PubMed: 16172383]

Kim J, Kundu M, Viollet B, Guan KL. AMPK and mTOR regulate autophagy through direct phosphorylation of Ulk1. Nature cell biology. 2011; 13:132–141. [PubMed: 21258367]

Kim JW, Dang CV. Cancer's molecular sweet tooth and the Warburg effect. Cancer research. 2006; 66:8927–8930. [PubMed: 16982728]

Kim YN, Koo KH, Sung JY, Yun UJ, Kim H. Anoikis resistance: an essential prerequisite for tumor metastasis. Int J Cell Biol. 2012; 2012:306879. [PubMed: 22505926]

LeBleu VS, O'Connell JT, Gonzalez Herrera KN, Wikman H, Pantel K, Haigis MC, de Carvalho FM, Damascena A, Domingos Chinen LT, Rocha RM, et al. PGC-1alpha mediates mitochondrial biogenesis and oxidative phosphorylation in cancer cells to promote metastasis. Nature cell biology. 2014; 16:992–1003. 1001–1015. [PubMed: 25241037]

Liang J, Mills GB. AMPK: a contextual oncogene or tumor suppressor? Cancer research. 2013; 73:2929–2935. [PubMed: 23644529]

Lin R, Elf S, Shan C, Kang HB, Ji Q, Zhou L, Hitosugi T, Zhang L, Zhang S, Seo JH, et al. 6-Phosphogluconate dehydrogenase links oxidative PPP, lipogenesis and tumour growth by inhibiting LKB1-AMPK signalling. Nat Cell Biol. 2015; 17:1484–1496. [PubMed: 26479318]

Luo Z, Zang M, Guo W. AMPK as a metabolic tumor suppressor: control of metabolism and cell growth. Future oncology. 2010; 6:457–470. [PubMed: 20222801]

Martinez Molina D, Jafari R, Ignatushchenko M, Seki T, Larsson EA, Dan C, Sreekumar L, Cao Y, Nordlund P. Monitoring drug target engagement in cells and tissues using the cellular thermal shift assay. Science. 2013; 341:84–87. [PubMed: 23828940]

Ng TL, Leprivier G, Robertson MD, Chow C, Martin MJ, Laderoute KR, Davicioni E, Triche TJ, Sorensen PH. The AMPK stress response pathway mediates anoikis resistance through inhibition of mTOR and suppression of protein synthesis. Cell Death Differ. 2012; 19:501–510. [PubMed: 21941369]

Owonikoko TK, Zhang G, Kim HS, Stinson RM, Bechara R, Zhang C, Chen Z, Saba NF, Pakkala S, Pillai R, et al. Patient-derived xenografts faithfully replicated clinical outcome in a phase II co-clinical trial of arsenic trioxide in relapsed small cell lung cancer. Journal of translational medicine. 2016; 14:111. [PubMed: 27142472]

Paoli P, Giannoni E, Chiarugi P. Anoikis molecular pathways and its role in cancer progression. Biochim Biophys Acta. 2013; 1833:3481–3498. [PubMed: 23830918]

Petit V, Massonnet G, Maciorowski Z, Touhami J, Thuleau A, Nemati F, Laval J, Chateau-Joubert S, Servely JL, Vallerand D, et al. Optimization of tumor xenograft dissociation for the profiling of cell surface markers and nutrient transporters. Laboratory investigation; a journal of technical methods and pathology. 2013; 93:611–621. [PubMed: 23459372]

Ponomarev V, Doubrovin M, Serganova I, Vider J, Shavrin A, Beresten T, Ivanova A, Ageyeva L, Tourkova V, Balatoni J, et al. A novel triple-modality reporter gene for whole-body fluorescent, bioluminescent, and nuclear noninvasive imaging. Eur J Nucl Med Mol Imaging. 2004; 31:740–751. [PubMed: 15014901]

Rungtabnapa P, Nimmannit U, Halim H, Rojanasakul Y, Chanvorachote P. Hydrogen peroxide inhibits non-small cell lung cancer cell anoikis through the inhibition of caveolin-1 degradation. Am J Physiol Cell Physiol. 2011; 300:C235–245. [PubMed: 21148404]

Sanchez-Cespedes M, Parrella P, Esteller M, Nomoto S, Trink B, Engles JM, Westra WH, Herman JG, Sidransky D. Inactivation of LKB1/STK11 is a common event in adenocarcinomas of the lung. Cancer research. 2002; 62:3659–3662. [PubMed: 12097271]

Schafer ZT, Grassian AR, Song L, Jiang Z, Gerhart-Hines Z, Irie HY, Gao S, Puigserver P, Brugge JS. Antioxidant and oncogene rescue of metabolic defects caused by loss of matrix attachment. Nature. 2009; 461:109–113. [PubMed: 19693011]

Shashidharan P, Michaelidis TM, Robakis NK, Kresovali A, Papamatheakis J, Plaitakis A. Novel human glutamate dehydrogenase expressed in neural and testicular tissues and encoded by an X-linked intronless gene. The Journal of biological chemistry. 1994; 269:16971–16976. [PubMed: 8207021]

Simpson CD, Anyiwe K, Schimmer AD. Anoikis resistance and tumor metastasis. Cancer letters. 2008; 272:177–185. [PubMed: 18579285]

Spandidos A, Wang X, Wang H, Seed B. PrimerBank: a resource of human and mouse PCR primer pairs for gene expression detection and quantification. Nucleic Acids Res. 2010; 38:D792–799. [PubMed: 19906719]

Steeg PS. Targeting metastasis. Nature reviews Cancer. 2016; 16:201–218. [PubMed: 27009393]

Sundararaman A, Amirtham U, Rangarajan A. Calcium-Oxidant Signaling Network Regulates AMP-activated Protein Kinase (AMPK) Activation upon Matrix Deprivation. The Journal of biological chemistry. 2016; 291:14410–14429. [PubMed: 27226623]

Toubal A, Clement K, Fan R, Ancel P, Pelloux V, Rouault C, Veyrie N, Hartemann A, Treuter E, Venteclef N. SMRT-GPS2 corepressor pathway dysregulation coincides with obesity-linked adipocyte inflammation. The Journal of clinical investigation. 2013; 123:362–379. [PubMed: 23221346]

Warburg O. On the origin of cancer cells. Science. 1956; 123:309–314. [PubMed: 13298683]

Weber GF. Metabolism in cancer metastasis. Int J Cancer. 2016; 138:2061–2066. [PubMed: 26355498]

Zaganas I, Spanaki C, Karpusas M, Plaitakis A. Substitution of Ser for Arg-443 in the regulatory domain of human housekeeping (GLUD1) glutamate dehydrogenase virtually abolishes basal activity and markedly alters the activation of the enzyme by ADP and L-leucine. The Journal of biological chemistry. 2002; 277:46552–46558. [PubMed: 12324473]

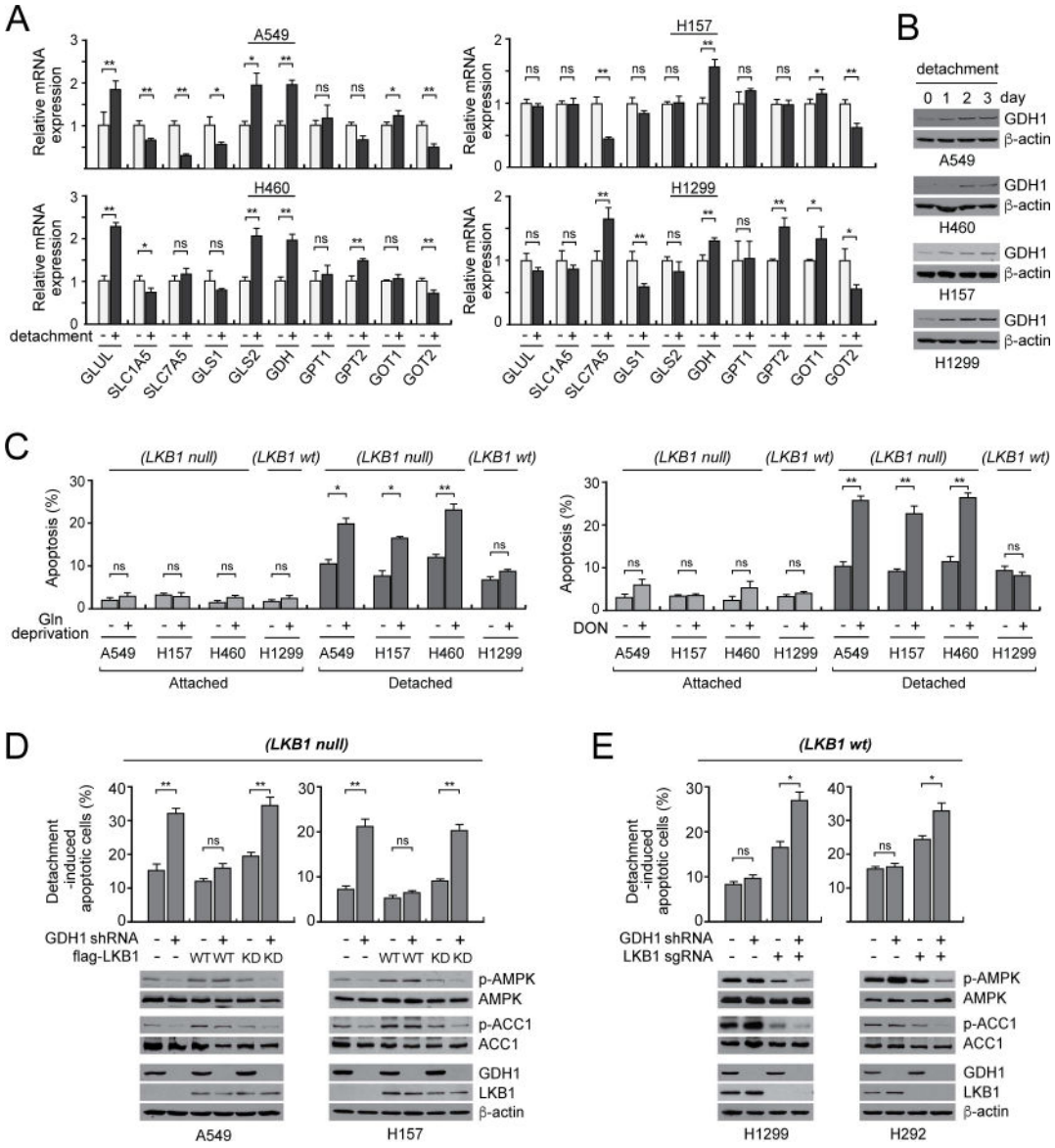

Figure 1. A glutaminolytic enzyme GDH expression is induced upon detachment and its contribution to anoikis resistance depends on LKB1 status in human lung cancers

(A) Relative RNA levels of glutaminolysis related enzymes and transporters in lung cancer cell lines after matrix detachment. Cells cultured under attached or detached conditions were applied to qRT-PCR. GAPDH was used as a control. **(B)** GDH1 protein level change upon anoikis induction was determined by western blot. **(C)** Effect of targeting glutaminolysis on detachment-induced cell death. Lung cancer cell lines were cultured attached or detached on 1% agar treated dishes in the presence or absence of glutamine (*left*) or 1 mM DON (*right*). Apoptotic cell death was determined by annexin V staining. LKB1 wt: LKB1 wild-type. **(D)** Effect of LKB1 overexpression on anoikis induction in LKB1 null cells with GDH1 knockdown. A549 and H157 cells were transfected with wild-type (WT) or kinase-dead (KD) K78I form of LKB1 and cultured under detached conditions. Anoikis (*top*) and phosphorylation of LKB1 downstream effectors AMPK and ACC1 (*bottom*) were measured

by annexin V staining and p-T172 AMPKα and p-S79 ACC1 western blot, respectively. **(E)** Effect of LKB1 knockout on anoikis induction in LKB1 wt cells with GDH1 knockdown. H1299 and H292 cells with LKB1 knockout were cultured under detached conditions. Anoikis induction and AMPK and ACC1 phosphorylation was assessed as in (D). Data are mean ± SD of three technical replicates and are representative of two independent biological experiments. Two-tailed Student's *t* test was used for statistics (ns: not significant; *: $0.01 < p < 0.05$; **: $p < 0.01$). See also Figure S1.

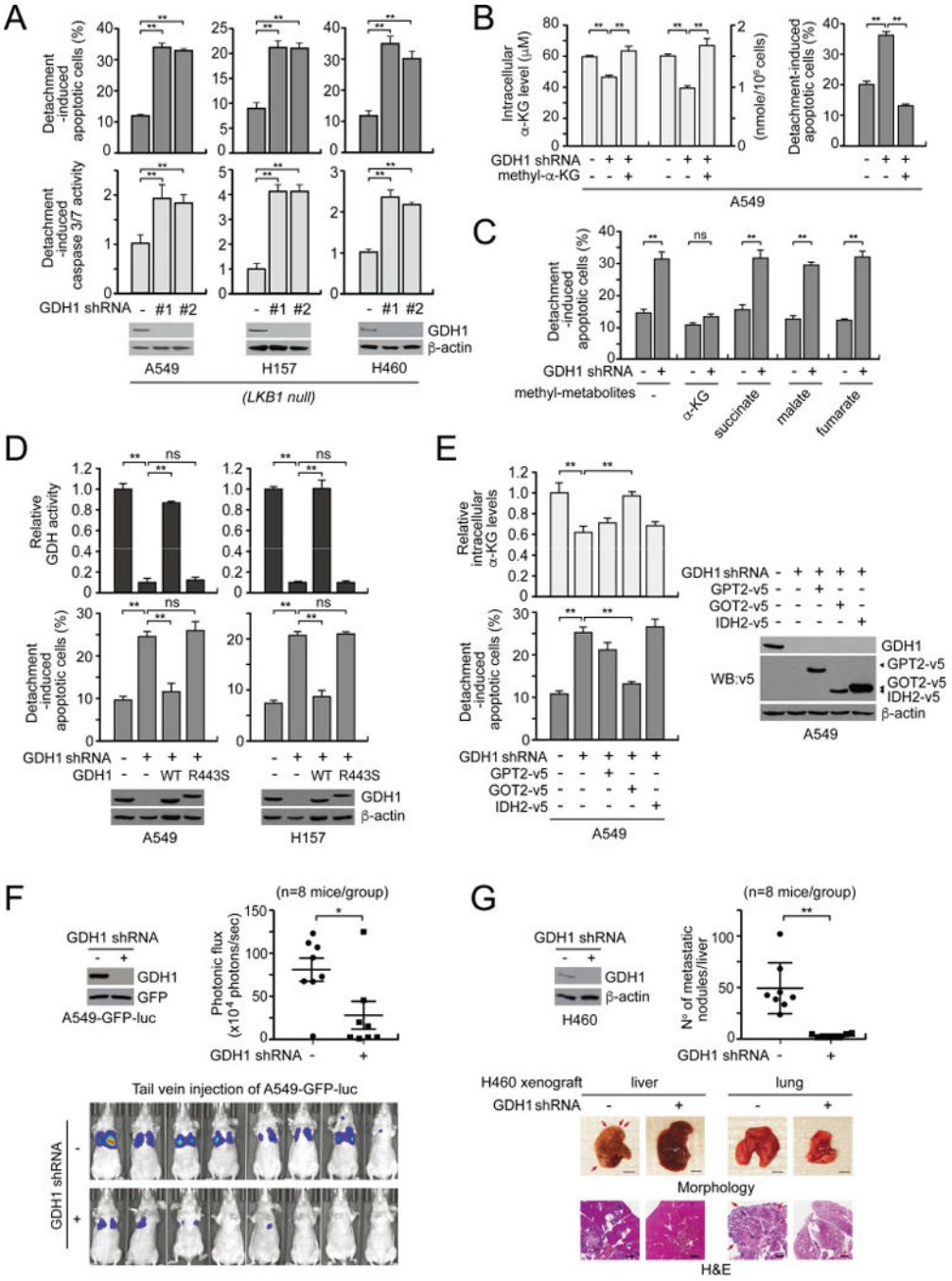

Figure 2. Loss of GDH1 and its product α-KG sensitizes LKB1-deficient lung cancer cells to anoikis induction and attenuates tumor metastasis *in vivo*

(A) Effect of GDH1 knockdown on detachment-induced apoptosis in a panel of LKB1 null lung cancer cells. Cells were cultured on 1% agar followed by annexin V staining (*top*) and caspase 3/7 activity assay (*bottom*). **(B)** Rescue effect of α-KG on anoikis resistance in A549 cells with GDH1 knockdown. Cells were cultured under detachment conditions in the presence and absence of methyl-αKG and intracellular α-KG level and anoikis were determined. **(C)** Effect of α-KG, succinate, malate, and fumarate on anoikis resistance of

GDH1 knockdown cells. Detached cells were cultured in the presence or absence of cell permeable metabolites, followed by annexin V staining. **(D)** Effect of shRNA-resistant GDH1 wild-type (WT) or enzyme-dead mutant GDH1 R443S expression on anoikis resistance in GDH1 knockdown cells. **(E)** Effect of α-KG producing enzymes GPT2, GOT2, and IDH2 on α-KG and anoikis in GDH1 knockdown cells. **(F–G)** Effect of GDH1 knockdown on tumor metastasis potential in A549 and H460 xenograft mice in an experimental metastasis model. Western blot analysis of GDH1 in injected A549-GFP-luciferase or H460 cells (*top left panels*). Nude mice were injected with A549-GFP-luciferase cells with or without GDH1 knockdown and average photonic flux and bioluminescence images of each group at week 7 are shown (F). NSG mice were injected with H460 cells harboring GDH1 shRNA or control vector and number of metastatic nodule in livers and representative liver and lung images of each group at day 18 are shown (G). Bars represent 5 mm for morphology and 1 mm for H&E staining. Data are mean ± SD of three technical replicates and are representative of three (A, C), four (B) or two (D and E) independent biological experiments. For (F-G), data are mean ± SEM and reflect a single cohort experiment (n=8). p values were determined by a two-tailed Student's *t* test (ns: not significant; *: $0.01 < p < 0.05$; **: $p < 0.01$). See also Figure S2.

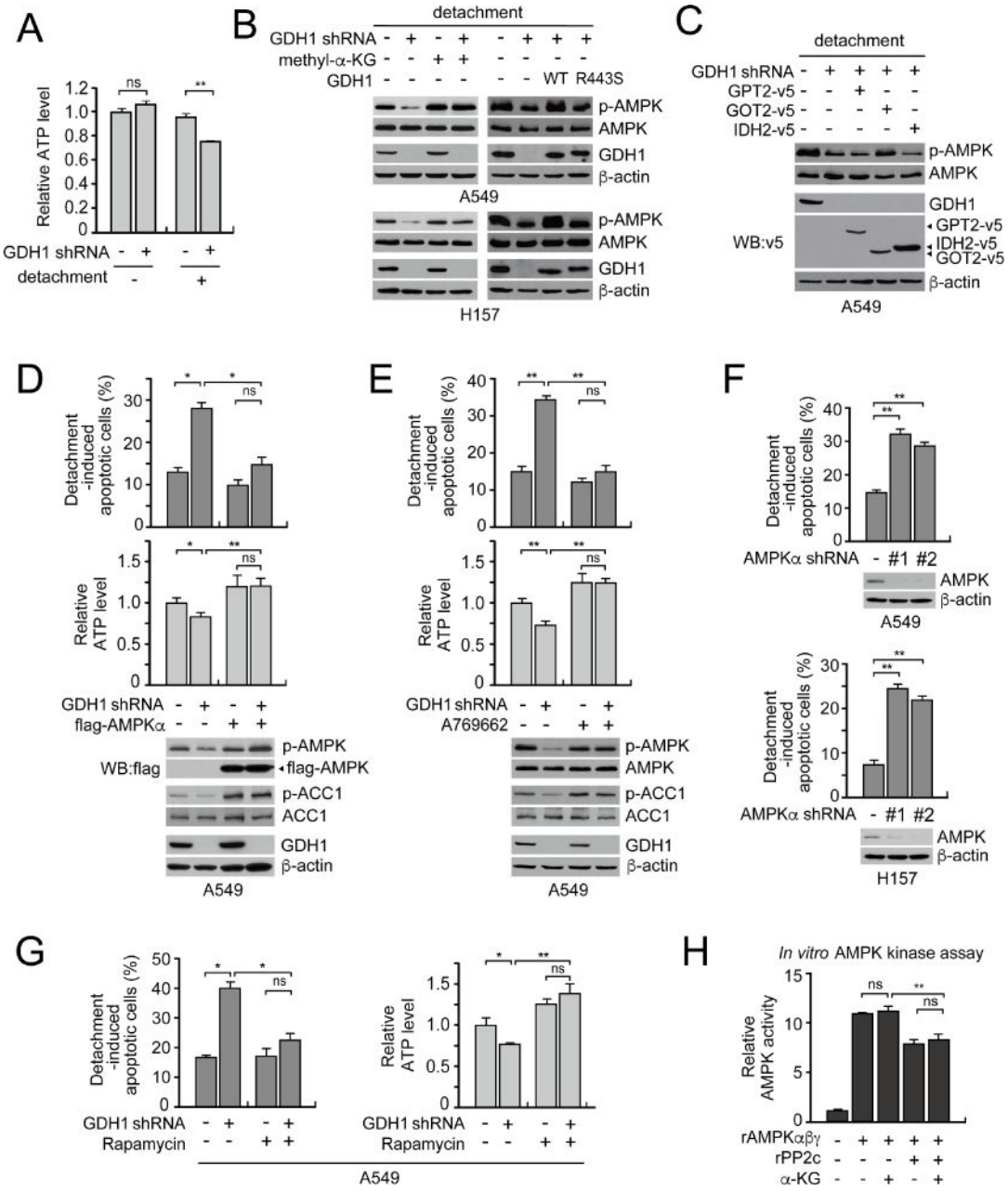

Figure 3. GDH1 confers anoikis resistance through AMPK activation and consequent energy regulation

(A) Effect of GDH1 knockdown on intracellular ATP levels upon detachment. **(B)** Effect of α-KG or rescue expression of shRNA-resistant GDH1 variants on AMPK activity in GDH1 knockdown cells. A549 and H157 cells with GDH1 knockdown were treated with methyl-αKG (*left*) or transfected with shRNA-resistant GDH1 WT or R443S vectors (*right*) and cultured under detachment conditions. **(C)** Overexpression of α-KG producing enzymes GPT2, GOT2, and IDH2 and their effect on AMPK activity. AMPK activity was assessed by AMPKα phosphorylation at T172 western blot. **(D-E)** Effect of AMPK restoration in detached GDH1 knockdown cells. A549 cells with GDH1 knockdown were transfected with

AMPKα (D) or treated with 100 μM of A769662 (E), and cultured under detached conditions followed by anoikis assay (*top*), ATP assay (*middle*), and western blot analysis of p-AMPKα and p-ACC1 (*bottom*). **(F)** Effect of AMPKα knockdown on anoikis induction in A549 and H157 cells. **(G)** Anoikis induction and ATP level changes in GDH1 knockdown cells treated with rapamycin (100 nM). **(H)** Effect of α-KG on AMPK kinase activity. Activity of recombinant AMPKαβγ in the presence of α-KG (50 μM) was assayed using SAMStide. To test the effect of α-KG on AMPK dephosphorylation, AMPK was incubated with recombinant PP2c in the presence or absence of α-KG, and AMPK activity was determined using SAMStide. Data are mean ± SD of three technical replicates and are representative of three (A, B, D-H) and two (C) independent biological experiments. p values were determined by a two-tailed Student's *t* test (ns: not significant; *: $0.01 < p < 0.05$; **: $p < 0.01$). See also Figures S3 and S4.

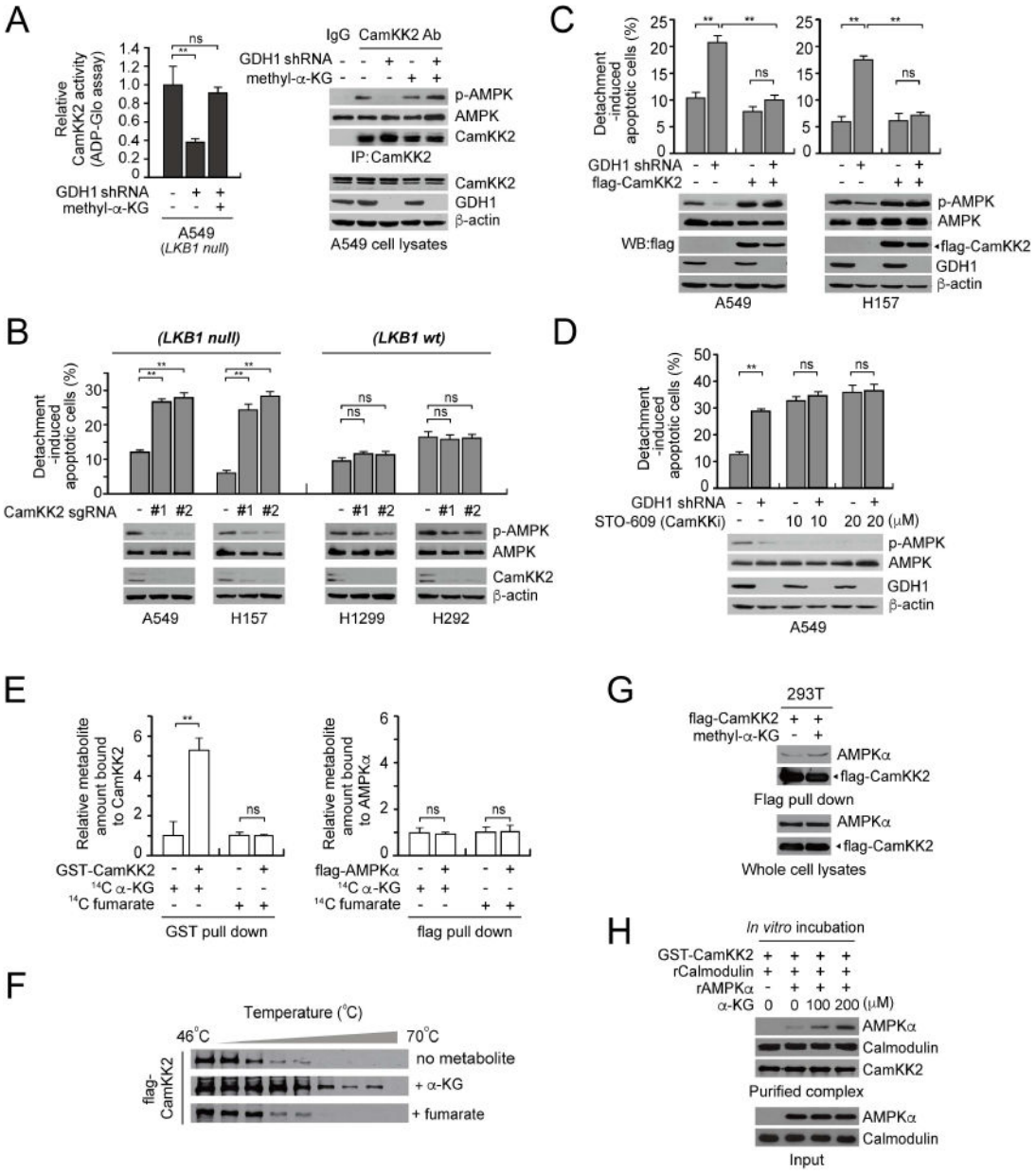

Figure 4. GDH1 contributes to anoikis resistance by regulating CamKK2 activity

(A) CamKK2 activity in A549 cells with GDH1 knockdown in the presence or absence of α-KG. A549 cells were cultured under detached conditions with methyl-α-KG prior to CamKK2 immunoprecipitation and kinase assay using AMPKα as a substrate. ADP-glo assay (*left*) and western blot of p-AMPKα T172 (*right*) were used to determine kinase activity of CamKK2. **(B)** Effect of transient CamKK2 knockout on AMPK activation and anoikis induction in LKB1 null or LKB1 wt cells. Anoikis and AMPK activity were assessed by annexin V staining and western blot analysis of p-T172 AMPKα, respectively. **(C)** Effect of flag-CamKK2 expression on AMPK activity and anoikis induction in LKB1 null cells with GDH1 knockdown. Detached cells with GDH1 knockdown were overexpressed with flag-CamKK2. **(D)** A549 with empty vector or GDH1 shRNA were

treated with increasing concentrations of STO-609 and cultured under detached conditions. Anoikis induction and AMPK activation were assessed as in (B) for (C) and (D). **(E)** Metabolite-protein binding assay. Purified GST-CamKK2 (*left*) or flag-AMPKα (*right*) from transfected 293T cells were incubated with radiolabeled α-KG or fumarate. CamKK2 or AMPKα bound α-KG or fumarate was quantified by scintillation counting. **(F)** Cellular thermal shift assay using flag-CamKK2 purified from 293T cells treated without or with dimethyl-α-KG or -fumarate. **(G)** α-KG enhances AMPK binding to CamKK2 in cells. Flag-CamKK2 was enriched from 293T cells treated with or without dimethyl-α-KG and CamKK2 bound endogenous AMPKα was detected by western blot. **(H)** α-KG enhances AMPK binding to CamKK2 *in vitro*. Bead-bound GST-CamKK2 was incubated with recombinant AMPKα and calmodulin in the presence of increasing concentrations of α-KG. Unbound proteins were washed away and retained AMPKα or calmodulin were assayed by western blot. Data are mean ± SD of three technical replicates and are representative of three (A-D) or two (E-H) independent biological experiments. p values were determined by a two-tailed Student's *t* test (ns: not significant; **: $p < 0.01$). See also Figure S5.

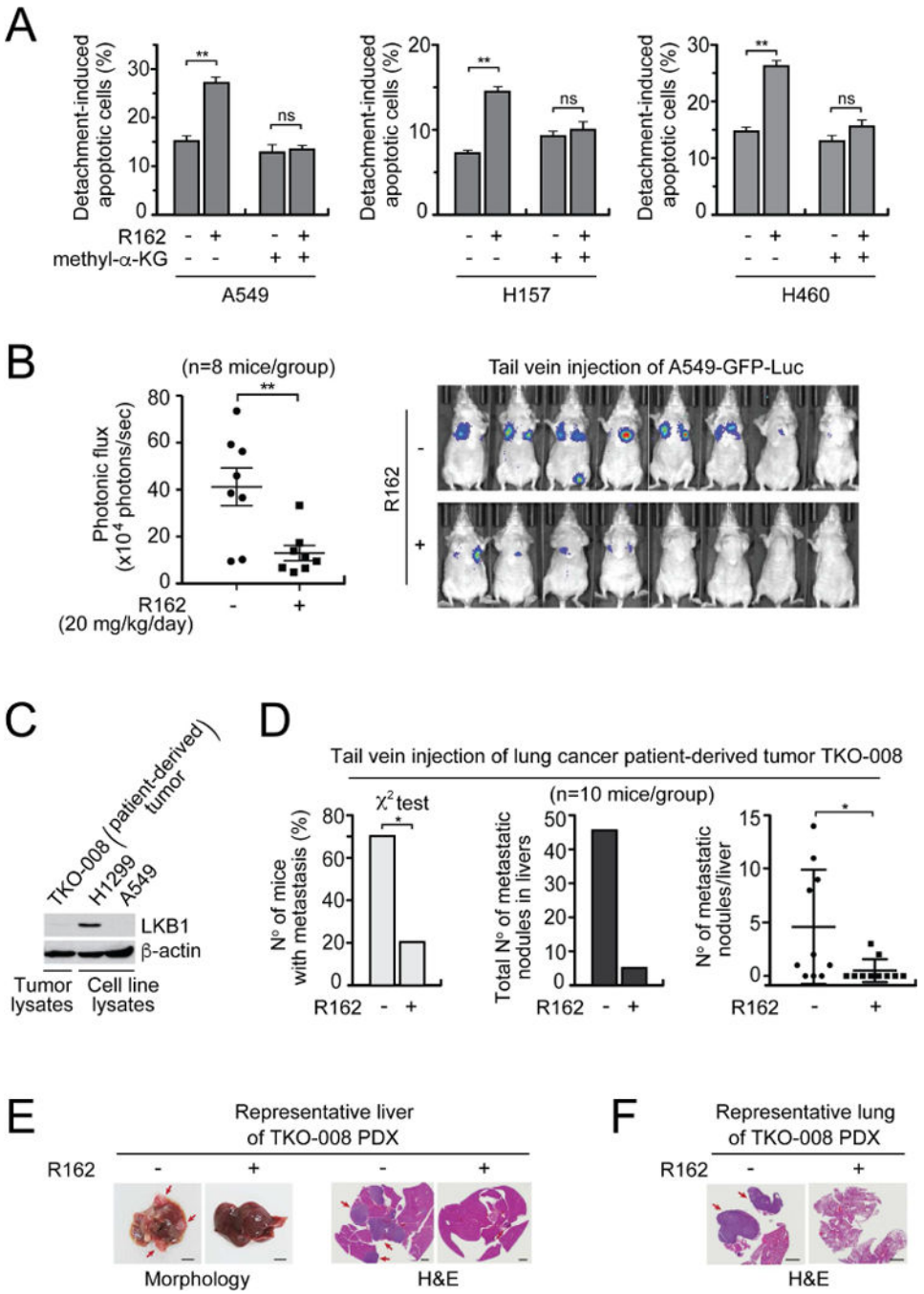

Figure 5. R162 treatment sensitizes LKB1-deficient NSCLC cells to anoikis and attenuates tumor metastasis in PDX mice

(A) LKB1-deficient cells were cultured under detached conditions in the presence or absence of R162 (20 or 40 μM) and methyl-α-KG (5 mM for A549 and H460, 1 mM for H157). Anoikis was determined by annexin V staining. **(B)** Effect of R162 on tumor metastasis in A549-luc xenograft mouse model. A549-luc cells with or without GDH1 knockdown were tail vein injected into nude mice. Average photonic flux and BLI of each group at week 10. **(C)** LKB1 status of lung cancer patient-derived tumor TKO-008. H1299

and A549 cells were used as controls. **(D)** R162 effect on experimental metastasis of lung cancer PDX. TKO-008 PDX tumor was single cell suspended and injected into the nude mice through the tail vein. The mice were treated with vehicle or R162 (20 mg/kg/day) from 1 day after xenograft for 45 days. Number of mice with metastasis (*left*), and numbers of metastatic nodules in the livers (*middle* and *right*) for each group are shown. **(E-F)** Representative images of livers (E) and lungs (F) of each PDX group are shown. Bars represent 5 mm for morphology and 2 mm for H&E staining. Data are mean ± SD of three technical replicates and are representative of three (A) independent biological experiments. For (B-D), data are mean ± SEM (B) or mean ± SD (D) and reflect a single cohort experiment (n=8 for B-C and n=10 for D). p values were determined by a chi-square test for (D) *left* and two-tailed Student's *t* test for the others (ns: not significant; *: $0.01 < p < 0.05$; **: $p < 0.01$). See also Figure S6.

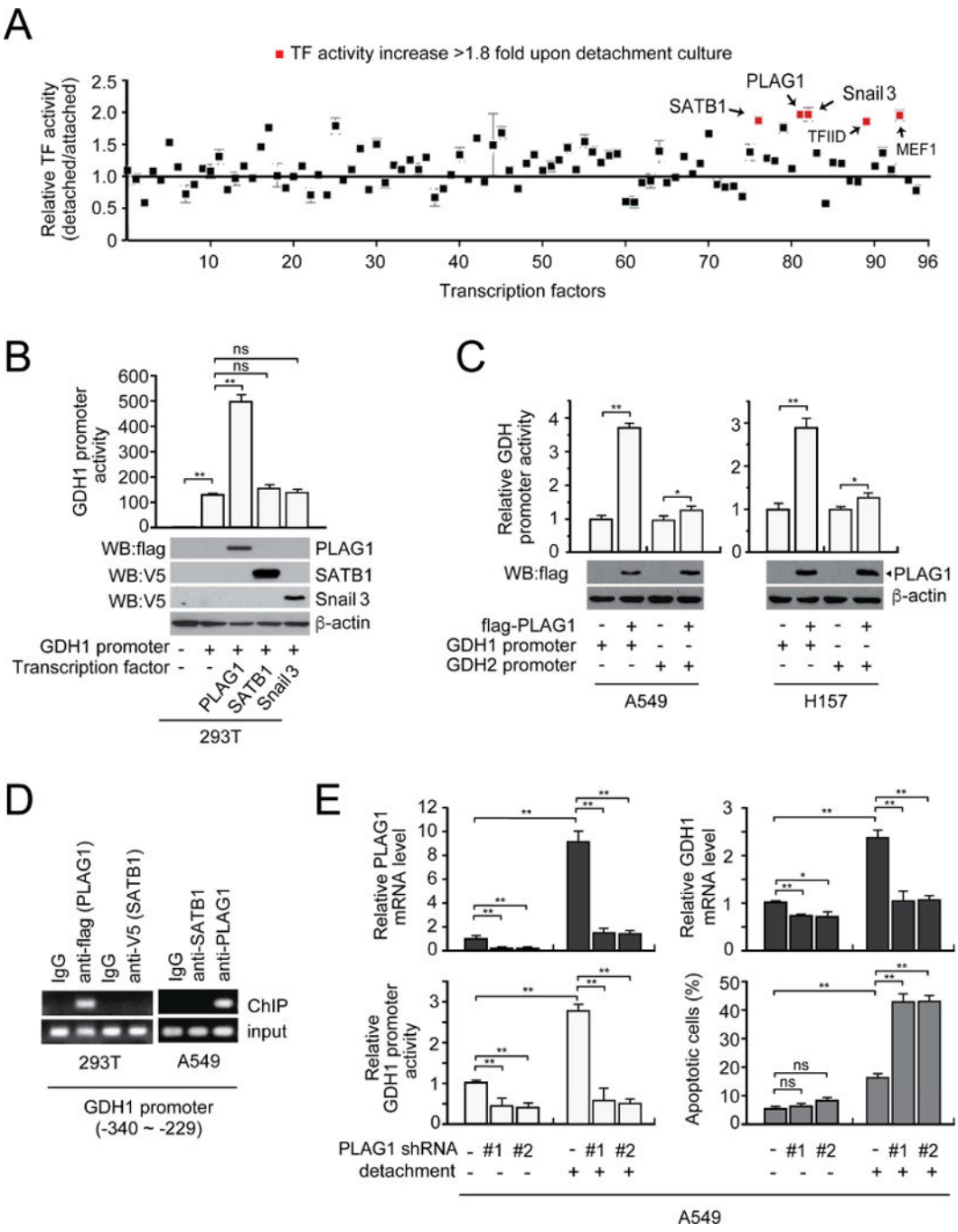

Figure 6. PLAG1 promotes GDH1 expression to confer anoikis resistance in human lung cancer

(A) Transcription factor profiling identified transcription factors whose activity is elevated in A549 cells in response to detachment. **(B)** GDH1 promoter activity in the presence of PLAG1, SATB1, or Snail3. **(C)** GDH1 and GDH2 promoter activity in the presence of PLAG1. **(D)** ChIP assay of PLAG1 or SATB1 binding to GDH1 promoter region. Antibodies against flag and V5 were used for 293T cells and anti-SATB1 and PLAG1 antibodies to enrich endogenous SATB1 and PLAG1 in A549 cells. **(E)** A549 cells expressing empty vector or PLAG1 shRNA clones were cultured under attached or detached

conditions and GDH1 mRNA level, GDH1 promoter activity, and apoptotic cell death were measured. PLAG1 knockdown was confirmed by qRT-PCR. Data are mean ± SD of three technical replicates and are representative of three (B and E) or two (C and D) independent biological experiments. p values were determined by two-tailed Student's *t* test for (B) and (D) (ns: not significant; **: $p < 0.01$).

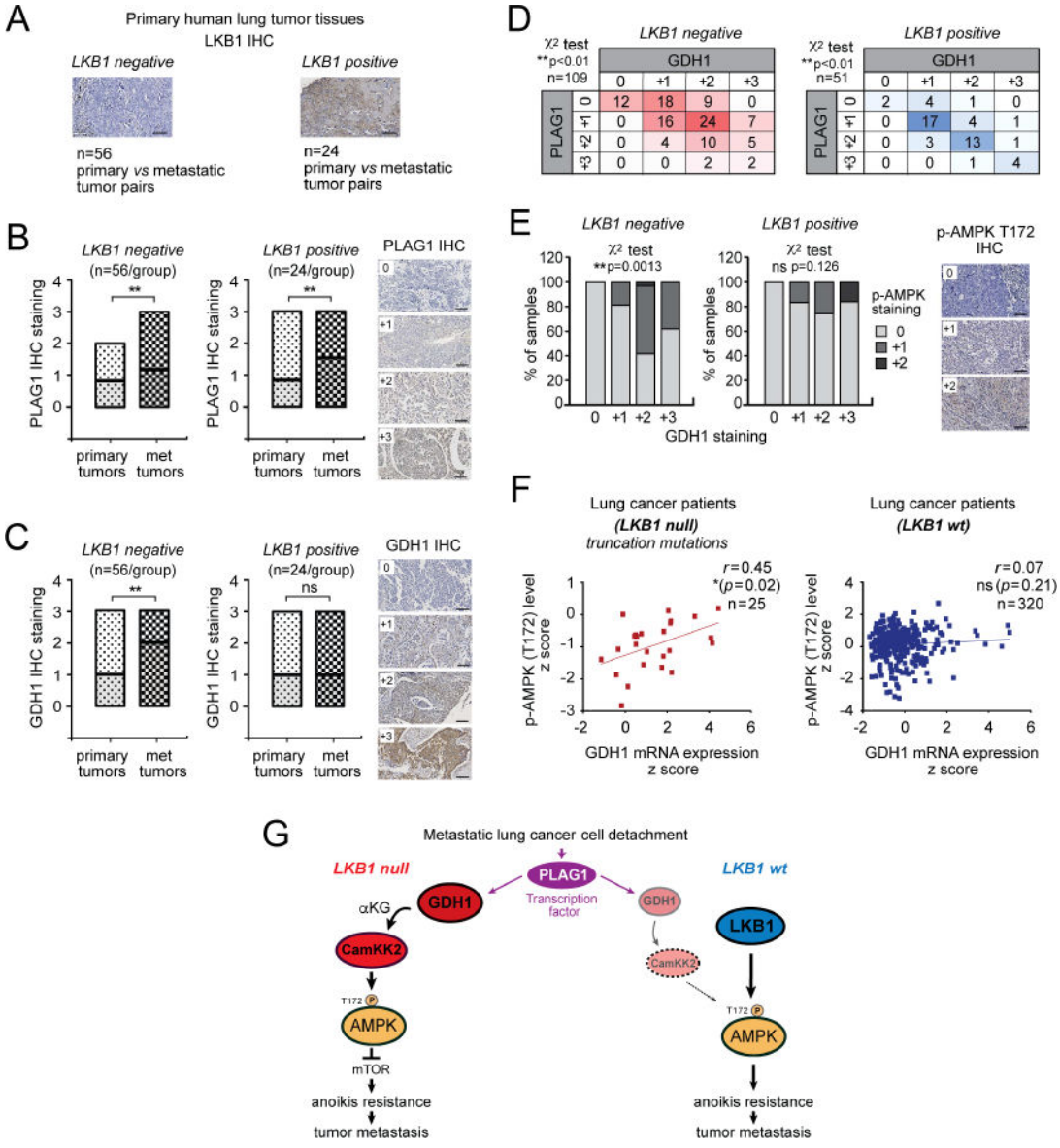

Figure 7. GDH1 signaling correlates with metastatic progression in human LKB1-deficient lung cancer

IHC analyses of PLAG1, GDH1, LKB1, and phospho-AMPK T172 using 80 paired primary and metastasized tumor tissues from patients with lung cancer. **(A)** Representative images of LKB1 negative and positive metastatic tumors are shown. Scale bars represent 100 μm. **(B-C)** The levels of PLAG1 (B) and GDH1 (C) in LKB1-negative (*left*) or -positive (*right*) primary and metastasized tumors from lung cancer patients were determined by IHC staining. Bars represent the min to max values, with lines at the median. Representative IHC staining images are shown on the right for 0~+3 scores. Scale bars represent 100 μm. **(D)** The correlations between PLAG1 and GDH1 in LKB1-negative and -positive groups. **(E)** The correlations between GDH1 and activation status of AMPK in LKB1-negative and -positive groups. AMPK activity was assessed by phospho-AMPKα T172 staining. Representative IHC images for phospho-AMPKα are presented on the right for 0, +1, and

+2 scores. Scale bars represent 100 μm. p values were determined by two-tailed paired Student's *t* test for (B) and (C), and chi-square test for (D) and (E)(ns: not significant; **: $p < 0.01$). **(F)** Correlation between z scores of phospho-AMPKα T172 expression and GDH1 mRNA expression in lung adenocarcinoma patient tumors with LKB1 loss by truncation mutations (*left*) or LKB1 wt (*right*). GDH1 mRNA expression z-scores (RNA Seq V2 RSEM), AMPKα T172 phospho-protein expression z-scores (RPPA), and LKB1 mutation status in TCGA Lung Adenocarcinoma were downloaded from cBioportal. Pearson correlation analysis was performed using Graphpad Prism 7.0. **(G)** Proposed model of GDH1-mediated anoikis resistance and tumor metastasis in lung cancer. GDH1 and α-KG are commonly upregulated by PLAG1 upon detachment in lung cancer cells. In LKB1 null cells, GDH1 activates CamKK2 leading to AMPK-mediated anoikis resistance and tumor metastasis, whereas in LKB1 wt harboring cells, LKB1 primarily controls AMPK activation and provides anoikis resistance and tumor metastasis in a GDH1-independent manner.